Isotopic mass fractionation laws for magnesium and their effects on 26Al–26Mg systematics in Solar System materials

Article *in* Geochimica et Cosmochimica Acta · February 2015

DOI: 10.1016/j.gca.2015.01.034

CITATIONS
5

READS
100

6 authors, including:

Philip E. Janney
University of Cape Town
114 PUBLICATIONS **2,645** CITATIONS
SEE PROFILE

Meenakshi Wadhwa
Arizona State University
292 PUBLICATIONS **4,177** CITATIONS
SEE PROFILE

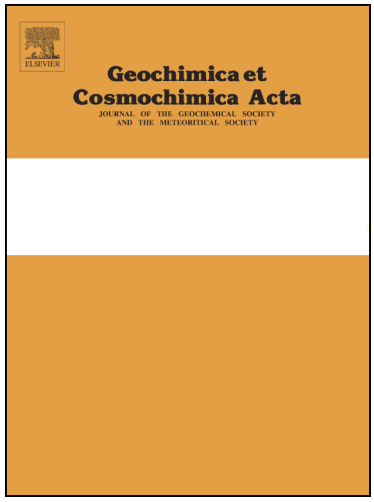

Isotopic mass fractionation laws for magnesium and their effects on ^{26}Al-^{26}Mg systematics in solar system materials

Andrew M. Davis, Frank M. Richter, Ruslan A. Mendybaev, Philip E. Janney, Meenakshi Wadhwa, Kevin D. McKeegan

PII: S0016-7037(15)00070-8
DOI: http://dx.doi.org/10.1016/j.gca.2015.01.034
Reference: GCA 9122

To appear in: *Geochimica et Cosmochimica Acta*

Received Date: 3 July 2014
Accepted Date: 27 January 2015

Please cite this article as: Davis, A.M., Richter, F.M., Mendybaev, R.A., Janney, P.E., Wadhwa, M., McKeegan, K.D., Isotopic mass fractionation laws for magnesium and their effects on ^{26}Al-^{26}Mg systematics in solar system materials, *Geochimica et Cosmochimica Acta* (2015), doi: http://dx.doi.org/10.1016/j.gca.2015.01.034

Isotopic mass fractionation laws for magnesium and their effects on ^{26}Al-^{26}Mg systematics in solar system materials

Andrew M. Davis[1,2,3], Frank M. Richter[1,3], Ruslan A. Mendybaev[1,3], Philip E. Janney[1,4,*], Meenakshi Wadhwa[1,4,§], and Kevin D. McKeegan[5]

[1]Chicago Center for Cosmochemistry, [2]Enrico Fermi Institute, [3]Department of the Geophysical Sciences, The University of Chicago, Chicago, Il 60637 (a-davis@uchicago.edu)

[4]Department of Geology, The Field Museum, Chicago, IL 60605.

[5]Department of Earth and Space Sciences, University of California, Los Angeles, CA 90095

*Present address: Department of Geological Sciences, University of Cape Town, Rondebosch 7701, South Africa.

[§]Present address: Center for Meteorite Studies, School of Earth and Space Exploration, Arizona State University, Tempe, AZ 85287

ABSTRACT

Magnesium isotope ratios are known to vary in solar system objects due to the effects of ^{26}Al decay to ^{26}Mg and mass dependent fractionation, but anomalies of nucleosynthetic origin must also be considered. In order to infer the amount of enhancement of ^{26}Mg/^{24}Mg due to ^{26}Al decay or to resolve small nucleogenetic anomalies, the exact relationship between ^{26}Mg/^{24}Mg and ^{25}Mg/^{24}Mg ratios due to mass-dependent fractionation, the mass-fractionation "law", must be accurately known so that the ^{25}Mg/^{24}Mg ratio can be used to correct the ^{26}Mg/^{24}Mg ratio for mass fractionation. Mass-dependent fractionation in mass spectrometers is reasonably well characterized, but not necessarily fully understood. It follows a simple power fractionation law, sometimes referred to as the "exponential law". In contrast, mass fractionation in nature, in particular that due to high temperature evaporation that likely caused the relatively large effects observed in calcium-, aluminum-rich inclusions (CAIs), is reasonably well understood, but mass-fractionation laws for magnesium have not been explored in detail. The magnesium isotopic compositions of CAI-like evaporation residues produced in a vacuum furnace indicate that the slope on a log ^{25}Mg/^{24}Mg vs. log ^{26}Mg/^{24}Mg plot is ~0.5128, and different from those predicted by any of the commonly used mass-fractionation laws. Evaporation experiments on forsterite-rich bulk compositions give exactly the same slope, indicating that the measured mass-fractionation law for evaporation of magnesium is applicable to a wide range of bulk compositions. We discuss mass-fractionation laws and the implications of the measured fractionation behavior of magnesium isotopes for ^{26}Al-^{26}Mg chronology.

1. INTRODUCTION

Excess ^{26}Mg from the decay of ^{26}Al was discovered in 1976, by thermal ionization mass spectrometry (TIMS) of mineral separates from a calcium-, aluminum-rich inclusion from the Allende CV3 chondrite (Lee et al., 1976). Since that time, the ^{26}Al-^{26}Mg system has been of great interest because of its potential for precise early solar system chronology. Until the 21st century, all of the data were generated by secondary ion mass spectrometry (SIMS) or TIMS using single-collector instruments; the data that most precisely defined the early solar system ^{26}Al/^{27}Al ratio were largely based on SIMS analyses of CAI minerals with high Al/Mg ratios. These studies established a "canonical" value of ~5×10^{-5} for the solar system (see review by

MacPherson et al., 1995). In the last decade, multicollector inductively coupled plasma mass spectrometry (MC-ICPMS) and multicollector secondary ion mass spectrometry (MC-SIMS) have made possible much higher precision magnesium isotopic analyses that provide chronologically useful data on low-Al/Mg phases in CAIs and in chondrules, and now allow study of the evolution of initial $^{26}Mg/^{24}Mg$ ratios (e.g., Villeneuve et al., 2009; MacPherson et al., 2012; Mishra and Chaussidon, 2014; see Davis and McKeegan, 2014, for a review).

Magnesium has three isotopes, 24, 25 and 26, which were apparently very well mixed in early solar system materials. Mass-independent isotopic anomalies can be difficult to recognize in magnesium, because of the decay of ^{26}Al. Except for demonstrably presolar grains (Zinner, 2014), there are no objects reported with large ^{26}Mg excesses unsupported by high Al/Mg ratios, but there are some CAIs with ^{26}Mg deficits of up to 5 ‰ that appear to be unrelated to the ^{26}Al-^{26}Mg system. Such anomalies have been found only in rare platy crystals of hibonite in CM chondrites (Ireland et al., 1991; Liu et al., 2009), the FUN inclusion EK1-4-1 (Wasserburg et al., 1977), and possibly the CAI Egg-3 (Wasserburg et al., 2012; see below). Magnesium isotope anomalies were reported in several other FUN inclusions, but these are likely the result of application of inappropriate mass fractionation laws; we address this issue below. Thus, it is generally considered that magnesium isotope ratios in normal solar system objects vary only due to the effects of ^{26}Al decay to ^{26}Mg and mass-dependent fractionation. In order to infer the amount of enhancement of $^{26}Mg/^{24}Mg$ due to ^{26}Al decay, the exact relationship between $^{26}Mg/^{24}Mg$ and $^{25}Mg/^{24}Mg$ ratios due to mass-dependent fractionation must be known so that the $^{25}Mg/^{24}Mg$ ratio can be used to correct the $^{26}Mg/^{24}Mg$ ratio for mass fractionation.

Mass-dependent fractionation can occur: (1) in nature; (2) during elemental separation and purification from synthetic and natural materials for isotopic analysis; and (3) in mass spectrometers. It is the first process that we are concerned with here. We cannot unambiguously prove how CAIs came to have mass-fractionated magnesium. However, the fact that the magnesium isotopic compositions of large igneous CAIs from CV chondrites are almost always heavy and, when silicon is measured, correlated with heavy silicon isotopic compositions (Clayton et al., 1988; Shahar and Young, 2007; Grossman et al., 2008; Larsen et al., 2011; Kita et al., 2012; MacPherson et al., 2012; Wasserburg et al., 2012; Bullock et al., 2013) is a strong indication that the process involved evaporation from a melt (Davis et al., 1990). Evaporation residues similarly enriched in the heavy isotopes of magnesium and silicon have been produced in laboratory experiments where CAI-like liquids were evaporated (Richter et al., 2002, 2007; Knight et al., 2009b; Mendybaev et al., 2013). Mass fractionation can also occur when magnesium is incompletely collected from ion exchange columns during chemical separation and purification, but most workers go to great lengths to prevent this effect. Mass spectrometers typically mass-fractionate magnesium (and other elements) relative to their true composition. Instrumental mass fractionation is especially prominent in ICPMS instruments, where effects for magnesium are typically 80–100 ‰ amu^{-1}. However, during solution ICPMS, samples and standards are all present in the same purified chemical form and instrumental mass fractionation is normalized away by sample-standard bracketing. In SIMS, mass fractionation can occur during sputtering and within the mass spectrometer; in laser ablation ICPMS, mass fractionation can occur during laser ablation and transport into the plasma torch, in addition to the fractionation within the ICP mass spectrometer. However, in both *in situ* techniques, mineral standards of similar chemical composition and known magnesium isotopic compositions are analyzed under the same experimental conditions as the samples, thereby normalizing the measured isotopic compositions and correct-

ing the instrumental mass fractionation. Although this method of "sample-standard bracketing" is not as well controlled as that practiced in solution ICPMS measurements, nevertheless when standards are run frequently, high reproducibility can result in high precision MC-SIMS and LA-MC-ICPMS measurements.

There has been a great deal of attention paid to isotopic fractionation effects in mass spectrometers, initially in TIMS, and later in MC-ICPMS and MC-SIMS, and a number of different fractionation "laws" have been derived (e.g., Schramm et al., 1970; Russell et al., 1978; Esat, 1984; Hart and Zindler, 1989; Habfast, 1998; Maréchal et al., 1999; Albarède et al., 2004; Albarède and Beard, 2004; Villeneuve et al., 2009; Bizzarro et al., 2011; Luu et al., 2013). Less attention has been paid to the fractionation laws appropriate in nature, with the exceptions of the Young et al. (2002) exploration of kinetic and equilibrium laws, and of measurements of calcium and titanium fractionation during evaporation (Zhang et al., 2014). Coarse-grained igneous CAIs, where most ^{26}Al-^{26}Mg studies are done, typically have mass-fractionation effects of a few ‰ amu^{-1} and a subset of these, the so-called FUN inclusions (named for their Fractionation and Unidentified Nuclear isotopic effects, Wasserburg et al., 1977), can have effects of a few tens of ‰ amu^{-1}. It is thought that these fractionation effects are caused by the kinetic isotope effect operating during high temperature evaporation of CAI precursors (e.g., Clayton et al., 1984; Grossman et al., 2000). Given the high precision currently achievable in magnesium isotope measurements, the law used to correct CAI data for natural mass fractionation effects can significantly affect the inferred amount of radiogenic ^{26}Mg, especially in cases where the degree of mass fractionation is large and/or the Al/Mg in the phase analyzed is relatively low. A variety of fractionation laws have been used to correct magnesium isotopic data. We review these laws, determine the law appropriate for magnesium from laboratory evaporation of melts of CAI composition, and examine the consequences for ^{26}Al-^{26}Mg chronology and for magnesium isotope anomalies in FUN CAIs.

2. MASS-FRACTIONATION LAWS

Mass-fractionation laws have been of considerable interest to analysts for many years, because the isotope ratios measured in mass spectrometers almost always differ from the true ratios. As there are a number of mass-fractionating processes that can occur in mass spectrometers (such as evaporation from a TIMS filament, diffusion within the residue on the TIMS filament, a variety of effects related to the interface between the 1 atm argon plasma source and the high vacuum of ICP mass spectrometers (Andrén et al., 2004), ionization during sputtering in SIMS, occultation of ion beams on slits within mass spectrometers, etc.), the primary approach has been to fit simple mathematical functions to data on standards for which there are variations in mass-dependent fractionation with time or with instrumental conditions. The laws that have been used to describe mass spectrometer behavior are typically not meant to convey physical understanding; instead, they are intended to provide a simple algorithm by which mass spectrometer data can be corrected for instrumental fractionation effects. The most widely used such law is the exponential law, which Russell et al. (1978) found best explained variations in calcium isotopic composition measured on standards in a TIMS, but a number of other laws have been proposed and used. Mass-fractionation laws governing magnesium isotopic fractionation in nature have been considered and relationships for equilibrium and kinetic fractionation have been proposed (Young et al., 2002; Young and Galy, 2004).

The exact masses of the three stable magnesium isotopes are 23.985041698 ± 0.000000014, 24.985836976 ± 0.000000050, and 25.982592968 ± 0.000000031 amu on the $^{12}C \equiv 12$ scale (Wang et al., 2012; note that the rounded version of the data table is found in this reference and the full, unrounded version can be found at http://amdc.impcas.ac.cn). These are atomic masses, and singly charged ions would differ in mass from these values by the mass of the electron (0.00055 amu). Such small mass differences do not matter when comparing mass fractionation processes in mass spectrometers, where singly charged ions are used, and nature, where neutral atoms predominate. However the differences between the exact masses and integer mass numbers do matter, at least to 0.001 amu, when dealing with fractionation laws at the precision currently attainable for magnesium isotopic measurements.

It is common to express magnesium isotope ratios using the familiar delta notation,

$$\delta^{25}\mathrm{Mg} = \left[\frac{\left(\frac{^{25}\mathrm{Mg}}{^{24}\mathrm{Mg}} \right)_{\mathrm{samp}}}{\left(\frac{^{25}\mathrm{Mg}}{^{24}\mathrm{Mg}} \right)_{\mathrm{std}}} - 1 \right] \times 1000; \quad (1)$$

δ^{26}Mg is similarly defined. Bizzarro et al. (2011) and subsequent papers from that group report μ^{25}Mg and μ^{26}Mg values, which are defined similarly to δ^{25}Mg and δ^{26}Mg, but the last factor is 10^6 rather than 1000. The standard now used in most ICPMS laboratories is DSM3, a solution made from pure magnesium from the Dead Sea Magnesium Company (Galy et al., 2003) that is close to average inner solar system magnesium isotopic composition. Several studies based on large numbers of chondrites and ocean island basalts, midocean ridge basalts, and mantle peridotites (Handler et al., 2009; Teng et al., 2010; Bourdon et al., 2010) have shown that the bulk silicate Earth has chondritic magnesium isotopic composition. All of these studies give compositions within error of one another; as an example, the DSM3-normalized values given by Teng et al. (2010) are δ^{25}Mg = –0.13±0.04‰ and δ^{26}Mg = –0.25±0.07‰ for the bulk silicate Earth and δ^{25}Mg = –0.15 ±0.04‰ and δ^{26}Mg = –0.28±0.06‰ for chondrites. A study by Chakrabarti and Jacobsen (2010) also shows that the bulk silicate Earth has chondritic magnesium isotopic composition, but the values they report for both the Earth and chondrites are isotopically lighter than those of other recent studies by 0.16 ‰ amu^{-1}. For SIMS, natural, unzoned minerals and glasses from high temperature terrestrial rocks are used and assumed to be of the same isotopic composition as the bulk silicate Earth and chondrites.

On three-isotope plots of δ^{25}Mg vs. δ^{26}Mg, mass-fractionation laws that depend linearly on mass difference, as well as mixtures between any pair of compositions, form straight lines. However, many mass-dependent isotopic fractionation processes operate in an exponential manner and therefore result in curves on a δ^{25}Mg vs. δ^{26}Mg plot. Hulston and Thode (1965) proposed the use of a three-isotope plot in which the logarithms of isotope ratios are plotted against one another. They introduced the δ' notation, which was adopted by Young et al. (2002) and Young and Galy (2004) for magnesium isotopes and is now widely used:

$$\delta^{25}\mathrm{Mg}' = 1000 \times \ln\left[\frac{\left(\frac{^{25}\mathrm{Mg}}{^{24}\mathrm{Mg}}\right)_{\mathrm{samp}}}{\left(\frac{^{25}\mathrm{Mg}}{^{24}\mathrm{Mg}}\right)_{\mathrm{std}}}\right]. \quad (2)$$

δ^{26}Mg′ is similarly defined. It is easy to convert δ' and δ values back and forth:

$$\delta^{25}\mathrm{Mg}' = 1000 \times \ln\left(\frac{\delta^{25}\mathrm{Mg}}{1000} + 1\right) \quad (3)$$

or

$$\delta^{25}\mathrm{Mg} = 1000 \times \left(e^{\frac{\delta^{25}\mathrm{Mg}'}{1000}} - 1\right). \quad (4)$$

δ- and δ'-values are very close to one another for small δ values. Exponential processes, including exponential, kinetic, equilibrium, and power fractionation laws, as well as Rayleigh fractionation, plot as straight lines on δ^{25}Mg′ vs. δ^{26}Mg′ plots, whereas linear fractionation laws and two-component mixtures lie along curves.

Whether plotted on δ^{25}Mg vs. δ^{26}Mg or δ^{25}Mg′ vs. δ^{26}Mg′ plots, all mass fractionation laws lie along approximately linear arrays with a slope of about one-half (Fig. 1). It is difficult to distinguish the various laws on such plots, so it is useful to choose one law as a standard of reference and plot differences in δ^{26}Mg or δ^{26}Mg′ between each law and the reference law vs. δ^{25}Mg′ (or δ^{25}Mg).

The most commonly used fractionation correction for high-precision analyses is the "exponential" law first proposed by Russell et al. (1978) Hart and Zindler (1989). This was the simple mathematical form that best described variations in isotopic composition from repeated measurements of a calcium standard with a TIMS as calcium evaporated from the filament (Russell et al., 1978; Hart and Zindler, 1989). This law was also found to adequately describe the behavior of sulfur (Papineau et al., 2005), calcium (Lundberg et al., 1994), and titanium (Fahey et al., 1987a) by SIMS. For magnesium, the exponential law is expressed as,

$$\frac{\left(\frac{^{25}\mathrm{Mg}}{^{24}\mathrm{Mg}}\right)_{\mathrm{samp}}}{\left(\frac{^{25}\mathrm{Mg}}{^{24}\mathrm{Mg}}\right)_{\mathrm{std}}} = \left(\frac{m_{25}}{m_{24}}\right)^{\phi} \quad (5)$$

and δ^{26}Mg*, which is the δ^{26}Mg value corrected for mass fractionation, is given by

$$\delta^{26}\mathrm{Mg}^{*} = \left[\frac{\left(\frac{^{26}\mathrm{Mg}}{^{24}\mathrm{Mg}} \right)_{\mathrm{samp}} \left(\frac{m_{26}}{m_{24}} \right)^{-\phi}}{\left(\frac{^{26}\mathrm{Mg}}{^{24}\mathrm{Mg}} \right)_{\mathrm{std}}} - 1 \right] \times 1000, \quad (6)$$

where the constants m_{24}, m_{25} and m_{26} are the exact masses of the magnesium isotopes. The parameter ϕ (called β in Russell et al., 1978, but renamed to avoid confusion as β is used later for another purpose in this paper) was calculated from Eq. 5 and applied to Eq. 6. On a plot of δ^{25}Mg´ vs. δ^{26}Mg´ (Fig. 1), the ϕ values are specific to individual points on a line whose slope is given by $\ln(m_{25}/m_{24})/\ln(m_{26}/m_{24}) = 0.51101$. This law is widely used in TIMS and MC-ICPMS and is frequently built into the manufacturer's data collection software. For CAI magnesium isotopic data, it is commonly used to correct for natural mass fractionation effects (e.g., Bizzarro et al., 2004; Jacobsen et al., 2008; Larsen et al., 2011). It should be emphasized that the exponential law has no theoretical basis; it is a simple mathematical function that, perhaps fortuitously, does a good job of describing the mass fractionation that occurs in many mass spectrometers. It also turns out that a perhaps oversimplified model of kinetic isotope fractionation gives the same mathematical relationship (Young et al., 2002; see below).

Since the exponential law is so widely used, we have chosen to take it as the standard of reference to compare with other fractionation laws. In Fig. 2, the differences between δ^{26}Mg calculated from various laws and δ^{26}Mg calculated from the exponential law are plotted vs. δ^{25}Mg.

The first paper reporting high-precision measurements of magnesium isotopic compositions of extraterrestrial materials, Schramm et al. (1970), made use of the following law to correct for mass fractionation:

$$\left(\frac{^{25}\mathrm{Mg}}{^{24}\mathrm{Mg}} \right)_{\mathrm{true}} = \frac{\left(\frac{^{25}\mathrm{Mg}}{^{24}\mathrm{Mg}} \right)_{\mathrm{meas}}}{1-\varepsilon} \quad (7)$$

and

$$\left(\frac{^{26}\mathrm{Mg}}{^{24}\mathrm{Mg}} \right)_{\mathrm{true}} = \frac{\left(\frac{^{26}\mathrm{Mg}}{^{24}\mathrm{Mg}} \right)_{\mathrm{meas}}}{\left(1-\varepsilon\right)^{2}}, \quad (8)$$

with δ^{26}Mg* calculated from $(^{26}\mathrm{Mg}/^{24}\mathrm{Mg})_{\mathrm{true}}$ and substituting the Catanzaro et al. (1966) value for terrestrial $^{25}\mathrm{Mg}/^{24}\mathrm{Mg}$ for $(^{25}\mathrm{Mg}/^{24}\mathrm{Mg})_{\mathrm{true}}$. This law gives a slope of 0.5000 on a plot of δ^{25}Mg´ vs. δ^{26}Mg´ (Fig. 1) and gives δ^{26}Mg* values that are higher than those given by the exponential law by ~0.044 ‰ per 1 ‰ of δ^{25}Mg (Fig. 2). This law was used by the Caltech group until the late 1970s (e.g., Lee and Papanastassiou, 1974; Lee et al., 1976; Wasserburg et al., 1977; Esat et al., 1978; Esat et al., 1979). Within the precision of the measurements, this law was adequate for normal CAIs, but may be problematic for FUN CAIs with large mass-fractionation effects (see below). Interestingly, Bizzarro et al. (2011) found that drift of magnesium isotopic

data on DSM3 within analytical sessions on their MC-ICPMS lies along a line of slope 0.5001±0.0012 on a plot of $\delta^{25}Mg'$ vs. $\delta^{26}Mg'$, which is quite close to the '70s Caltech law.

Russell et al. (1978) introduced a slightly different law they called the "power" law, which was more simply expressed by Esat (1984) and Hart and Zindler (1989). This law does not fit TIMS data for calcium isotopes well, but is among the mass-fractionation laws commonly discussed. Stated for magnesium, it is

$$\frac{\left(\frac{^{26}Mg}{^{24}Mg}\right)_{true}}{\left(\frac{^{26}Mg}{^{24}Mg}\right)_{meas}} = \left[\frac{\left(\frac{^{25}Mg}{^{24}Mg}\right)_{true}}{\left(\frac{^{25}Mg}{^{24}Mg}\right)_{meas}}\right]^{\frac{m_{26}-m_{24}}{m_{25}-m_{24}}}. \quad (9)$$

This law gives a slope of $(m_{25}–m_{24})/(m_{26}–m_{24}) = 0.50101$ on a plot of $\delta^{25}Mg'$ vs. $\delta^{26}Mg'$ (Fig. 1) and gives $\delta^{26}Mg^*$ values that are higher than those given by the exponential law by ~0.040 ‰ per 1 ‰ of $\delta^{25}Mg$ (Fig. 2). Note that for the power law, use of integer mass numbers of the magnesium isotopes (rather than exact masses), gives $\beta = 0.50000$, the slope obtained in Eqs. 7 and 8 and used in '70s Caltech law.

The simplest law used for correction of mass fractionation data is the "linear" law:

$$\delta^{26}Mg^* = \delta^{26}Mg_{meas} - \delta^{25}Mg_{meas} / 0.5. \quad (10)$$

This law was commonly used for SIMS data on high Al/Mg phases prior to the high precision era. For typical precision of 1–2 ‰ and $\delta^{25}Mg \leq 70$ ‰ (even FUN CAIs have $\delta^{25}Mg \leq 35$ ‰), this law is not significantly different from the exponential law (Fig. 2). At low values of $\delta^{25}Mg$, it gives results quite close to the power law, but it curves towards the exponential fractionation law, eventually crossing it at $\delta^{25}Mg = 47$ ‰. Hutcheon (1982) expressed the linear fractionation law in a different way:

$$\left(\frac{^{26}Mg}{^{24}Mg}\right)_{corr} = \left(\frac{^{26}Mg}{^{24}Mg}\right)_{meas} + \frac{1}{0.454}\left[\left(\frac{^{25}Mg}{^{24}Mg}\right)_{std} - \left(\frac{^{25}Mg}{^{24}Mg}\right)_{meas}\right], \quad (11)$$

where "corr" indicates the fractionation-corrected ratio, "meas" indicates ratios measured on unknown samples, and "std" indicates the terrestrial $^{25}Mg/^{24}Mg$ ratio, 0.12663 (Catanzaro et al., 1966). Although Hutcheon (1982) determined the slope of 0.454 from a plot of $^{25}Mg/^{24}Mg$ vs. $^{26}Mg/^{24}Mg$ for terrestrial standards measured by SIMS, this slope corresponds to a slope of exactly 0.5 on a plot of $\delta^{25}Mg$ vs. $\delta^{26}Mg$.

Closely related laws,

$$\delta^{26}Mg^* = \delta^{26}Mg_{meas} - \delta^{25}Mg_{meas} / \theta, \quad (12)$$

have been applied to MC-ICPMS data, where θ is the slope for a variety of measurements of terrestrial samples on a $\delta^{25}Mg$ vs. $\delta^{26}Mg$ plot, with $\theta = 0.5163$ (Galy et al., 2000) and $\theta = 0.5189$ (Galy et al., 2004). The latter value gives a fractionation law that is quite close to equilibrium

fractionation (see below; Fig. 2) for low values of δ^{25}Mg, which is perhaps not surprising for terrestrial samples, but curves away from other laws sharply with higher δ^{25}Mg.

Young et al. (2002) and Young and Galy (2004) have discussed equilibrium and kinetic mass dependent isotopic fractionation laws for magnesium. Fractionation factors for the magnesium isotopes can be defined:

$$\kappa_{25/24} = \frac{\left(\frac{^{25}\mathrm{Mg}}{^{24}\mathrm{Mg}}\right)_a}{\left(\frac{^{25}\mathrm{Mg}}{^{24}\mathrm{Mg}}\right)_b} \quad \text{and} \quad \kappa_{26/24} = \frac{\left(\frac{^{26}\mathrm{Mg}}{^{24}\mathrm{Mg}}\right)_a}{\left(\frac{^{26}\mathrm{Mg}}{^{24}\mathrm{Mg}}\right)_b}, \tag{13a,b}$$

where a and b refer to different phases or conditions. An equilibrium isotopic fractionation law has been derived for sulfur (Huston and Thode, 1965) and oxygen (Matsuhisa et al., 1978). Young et al. (2002) gave an expression for equilibrium fractionation, which Young and Galy (2004) used for equilibrium fractionation of magnesium isotopes:

$$\frac{\ln \kappa_{25/24}}{\ln \kappa_{26/24}} = \frac{\left(\frac{1}{m_{24}} - \frac{1}{m_{25}}\right)}{\left(\frac{1}{m_{24}} - \frac{1}{m_{26}}\right)}, \tag{14}$$

where m_{24}, m_{25} and m_{26} are the exact masses of the magnesium isotopes. Young and Galy (2004) rearranged this expression to give

$$\kappa_{25/24} = \kappa_{26/24}^{\beta}, \tag{15}$$

where

$$\beta = \frac{\left(\frac{1}{m_{24}} - \frac{1}{m_{25}}\right)}{\left(\frac{1}{m_{24}} - \frac{1}{m_{26}}\right)}. \tag{16}$$

This equation for equilibrium isotopic fractionation gives a slope of $\beta = 0.52100$ on a plot of δ^{25}Mg′ vs. δ^{26}Mg′ (Fig. 1) and gives δ^{26}Mg* values that are higher than those given by the exponential law by ~0.038 ‰ per 1 ‰ of δ^{25}Mg (Fig. 2).

Young et al. (2002) also proposed an expression for kinetic isotope fractionation, for which

$$\beta = \frac{\ln\left(\frac{m_{24}}{m_{25}}\right)}{\ln\left(\frac{m_{24}}{m_{26}}\right)} \tag{17}$$

is used in Eq. 15. Equation 17 is exactly the same as the one used to calculate the slope of the exponential law on a plot of δ^{25}Mg′ vs. δ^{26}Mg′. In the case of kinetic fractionation, use of the

exact masses of the magnesium isotopes may represent the maximum value of β, because molecular masses should be used for transport processes involving molecules. However, reduced masses should be used for cases where the rate-limiting step involves vibrations in a condensed phase. Since reduced masses are always lower than atomic masses, this would increase β above the value calculated from atomic masses. Using the masses of the magnesium isotopes, since silicate melts evaporate magnesium as Mg atoms (Nichols et al., 1995; Wang et al., 1999, 2001), the Young and Galy (2004) kinetic law gives a slope of $\beta = 0.51101$ on a plot of $\delta^{25}Mg'$ vs. $\delta^{26}Mg'$, exactly the same as the exponential law. Using molecular or reduced masses would give lower and higher values of the slope, respectively. Young et al. (2002) stated that the kinetic and equilibrium laws gave slopes of 0.510 and 0.520. These values are 0.001 lower than the values we give, because they used the mass numbers, A, of the magnesium isotopes, rather than the exact masses. Bizzarro et al. (2011) wrote that the kinetic law can be expressed as a form of Eq. 12,

$$\mu^{26}Mg^* = \mu^{26}Mg - \mu^{25}Mg / 0.511 \quad \text{(their Eq. 3)}, \tag{18}$$

but this is obviously incorrect and it is clear from subsequent publications that they did not use this law. Luu et al. (2013) wrote a similar equation early in their paper but used a correct equation later in their paper.

Evaporation of silicate and CAI-like melts yields data that are well described by the Rayleigh fractionation law (e.g., Davis et al., 1990; Wang et al., 2001; Richter et al., 2002; Richter et al., 2007; Mendybaev et al., 2013). This law applies to situations where the residue is continuously well mixed during evaporation and recondensation is negligible. Such a situation can be achieved in a well-designed laboratory experiment. Rayleigh fractionation also applies in nature, where many CAIs appear to have experienced evaporative mass loss while molten (Grossman et al., 2000; Richter et al., 2002; Richter et al., 2007; Grossman et al., 2008) under conditions where the surrounding gas pressure was sufficiently low such that recondensation was negligible and where diffusion in the melt was sufficiently fast to keep the residue effectively homogeneous.

The following form of the Rayleigh equation describes fractionation of a pair of isotopes:

$$\frac{R_{ij}}{R_{ij,0}} = \left[\frac{N_j}{N_{j,0}}\right]^{\alpha_{ij}-1}, \tag{19}$$

where species i is ^{25}Mg or ^{26}Mg, species j is ^{24}Mg, $R_{ij} = {}^{25}Mg/{}^{24}Mg$ or $^{26}Mg/^{24}Mg$, $R_{ij,0}$ is the same ratio initially present, N_j is the amount of ^{24}Mg remaining, $N_{j,0}$ is the amount of ^{24}Mg initially present, and α_{ij} is the ratio of the fluxes of the two isotopes away from the surface (see Richter, 2004, for a derivation and discussion of the conditions required for this equation to be applied to evaporation residues). The kinetic isotope fractionation factor α_{ij} is given by $\left(\gamma_i / \gamma_j\right)\sqrt{m_j / m_i}$, where γ_i and γ_j are the sticking coefficients of each isotope, a measure of the kinetic hindrance of evaporation, and m_i and m_j are the masses of the dominant gas species that would be in equilibrium with the melt, which in the case of magnesium are Mg atoms (Wang et al., 1999; Grossman et al., 2000). It has often been assumed that the kinetic hindrance of evaporation is the same for all isotopes of an element, so $\gamma_i = \gamma_j$ and $\alpha_{ij} = \sqrt{m_j / m_i}$ (e.g., Grossman et al., 2000, 2002). In their review of the ^{26}Al-^{26}Mg record in the solar system, MacPherson et al.

(1995) discussed fractionation laws as applied to magnesium, noted the inadequacy of the linear fractionation law commonly used at that time, and suggested that since Rayleigh fractionation of Mg atoms described fractionations in FUN inclusions fairly well, this law should be used to correct CAI data. We use the term "ideal" Rayleigh law, where α_{ij} is calculated from the exact masses of the magnesium isotopes and equal sticking coefficients are assumed for all isotopes, $\gamma_i = \gamma_j$. The ideal Rayleigh law gives a slope of $\beta = 0.51600$ on a plot of $\delta^{25}Mg'$ vs. $\delta^{26}Mg'$ (Fig. 1) and gives $\delta^{26}Mg^*$ values that are higher than those given by the exponential law by ~0.019 ‰ per 1 ‰ of $\delta^{25}Mg$ (Fig. 2).

As Richter et al. (2002, 2007) and Knight et al. (2009) have shown, the ideal Rayleigh law does not accurately describe the mass fractionation behavior during evaporation of CAI melts, at least for magnesium and silicon, because the measured α_{ij} values are closer to 1 than is predicted by the ideal Rayleigh law. We now explore the consequences of measured α_{ij} values for the mass fractionation law. Rather than $\left(\gamma_i / \gamma_j\right)\sqrt{m_j / m_i}$, as above, the flux ratios α_{ij} can be expressed as functions of the mass ratios of the isotopes,

$$\alpha_{ij} = \left(\frac{m_j}{m_i}\right)^{\xi}, \tag{20}$$

in order to take into account any differences in the kinetic hindrances γ_i among the isotopes. If we write Eq. 20 for the $^{25}Mg/^{24}Mg$ and $^{26}Mg/^{24}Mg$ ratios, take the natural logarithm of each, and divide the expression for $^{25}Mg/^{24}Mg$ by the one for $^{26}Mg/^{24}Mg$, we come up with the following expression for the slope of the $\delta^{25}Mg'$ vs. $\delta^{26}Mg'$ plot,

$$\frac{\delta^{25}Mg'}{\delta^{26}Mg'} = \frac{\alpha_{25,24} - 1}{\alpha_{26,24} - 1} = \frac{\left(\frac{m_{24}}{m_{25}}\right)^{\xi} - 1}{\left(\frac{m_{24}}{m_{26}}\right)^{\xi} - 1}. \tag{21}$$

By parameterizing α_{ij} in this way, we are assuming that the sticking coefficients γ_i are different for different isotopes and that they are related to one another by some power of the ratio of isotope masses. For the ideal Rayleigh law, $\xi = 0.5$, and the slope on the $\delta^{25}Mg'$ vs. $\delta^{26}Mg'$ plot is 0.51600, as above. However, Richter et al. (2007) measured $\alpha_{25,24}$ values as a function of temperature over the range 1600–1900°C and extrapolated to the value expected for CAI evaporation, near the liquidus at ~1400°C. Using their average $\alpha_{25,24}$ value over all experiments, 0.98704±0.00025, we calculate a ξ value of 0.316 and predict that the slope (β) on the $\delta^{25}Mg'$ vs. $\delta^{26}Mg'$ plot will be 0.51420±0.00006. Using their extrapolated value (0.99100) for an assumed CAI evaporation temperature of 1400°C, we predict a β value of 0.51322.

Maréchal et al. (1999) describe a generalized power law as a convenient way to represent a number of exponential-type fractionation laws; Wombacher and Rehkämper (2003) explicitly give the value for β in Eq. 15 for various laws. For magnesium, the value of β is given by

$$\beta = \frac{m_{24}^n - m_{25}^n}{m_{24}^n - m_{26}^n}, \quad (22)$$

where the m values are the exact masses of the magnesium isotopes. For the equilibrium law, n = –1 (β = 0.52100; see Eq. 16); for the power law, n = 1 (β = 0.50101; see the exponent in Eq. 9); the kinetic or exponential law is approached as n approaches 0 and a value of n = 10^{-6} (β = 0.51101) effectively represents this law; and the ideal Rayleigh law corresponds to n = –0.5 (β = 0.51600; rearrange the right side of Eq. 21 with ξ = 0.5). Note that for the power law, with n = 1 and integer mass numbers of the magnesium isotopes (rather than exact masses), β = 0.50000, the slope obtained in Eqs. 7 and 8 and used in '70s Caltech law.

The different fractionation laws are compared in Fig. 2, where deviations from the exponential law are plotted vs. δ^{25}Mg. Note that all of the power-type laws give lines that are very slightly curved, because differences in δ^{26}Mg (not δ^{26}Mg′) are plotted vs. δ^{25}Mg (not δ^{25}Mg′). It can be seen that for typical δ^{25}Mg values for CAIs of 5–10 ‰, the different laws will give δ^{26}Mg* values that differ by of several tenths of a ‰, variations that are significantly larger than the currently achievable precision of a few thousandths of a ‰ (e.g., Villeneuve et al., 2009; Bizzarro et al., 2011; Larsen et al., 2011; Olsen et al., 2013), which makes application of the most accurate and appropriate fractionation law all the more critical. As we will see in the next section, magnesium isotopic fractionation of residues from vacuum evaporation of melts of CAI composition is best described by a measured Rayleigh fractionation law that does not match any of the laws discussed above.

3. EXPERIMENTS

Richter et al. (2007) reported results of a series of vacuum evaporation experiments on melts of Type B CAI bulk composition that determined the relationship between degree of magnesium loss and magnesium isotopic composition. We will use data from the same experiments to examine mass fractionation laws. Magnesium isotopic compositions were measured by solution MC-ICPMS. Richter et al. (2007) only reported data for δ^{25}Mg; we report δ^{26}Mg and compare the results with the fractionation laws discussed above. Davis et al. (2005) examined mass fractionation laws using preliminary data. The data reported here are more complete, but do not alter the main conclusion that the observed fractionation effects can be described by the generalized power law with a fractionation behavior intermediate between those that have been suggested as representing kinetic and equilibrium fractionation laws and different from the ideal Rayleigh law.

In the experiments of Richter et al. (2007), samples with an initial bulk composition of 11.5 wt% MgO, 46.0 wt% SiO_2, 19.4 wt% Al_2O_3 and 23.1 wt% CaO were evaporated in a vacuum furnace at temperatures of 1600 to 1900°C for a variety of run times that led to magnesium losses of ~0 to ~99 %. The starting composition is similar to that expected if Type B CAIs typical of CV chondrites had lost a few tens of percent of their initial MgO and SiO_2 contents. Each residue quenched to a glass and was split. Half was mounted in epoxy and polished and the chemical composition was measured by energy-dispersive x-ray microanalysis with a scanning electron

microscope and the other half was crushed, dissolved in HF-HNO_3, and purified by cation exchange chromatography (Richter et al., 2007). Isotopic compositions were measured by sample-standard bracketing by using a Micromass IsoProbe MC-ICPMS at the Field Museum of Natural History. The running standards for isotopic measurements were the NIST magnesium solution SRM 980 from 2002 to mid-2004 and DSM3 from mid-2004 through 2006, but we restrict ourselves to the DSM3-normalized data, because of instrument instability problems in earlier data that are described in detail by Richter et al. (2007). Of the samples reported by Richter et al. (2007), only one, R2-16, was bracketed with SRM 980, not DSM3. Although there is nothing anomalous about that sample compared to others in the Richter et al. (2007), we do not include it in our data set for reasons of consistency. Isotope ratios are reported relative to the isotopic composition of R-13, a "zero-time" sample that was heated to 1800°C in the vacuum furnace and immediately quenched to a glass. This sample was determined to have the same chemical composition as the starting material and to be chemically uniform. The isotopic composition of R-13 was measured in every session where other evaporation residue samples were analyzed.

4. RESULTS

On the DSM3 scale, the magnesium isotopic composition of the zero-time sample, R-13, is $\delta^{25}Mg = -1.785 \pm 0.014$ ‰ and $\delta^{26}Mg = -3.520 \pm 0.026$ ‰ (2σ standard error), based on 34 analyses; errors in $\delta^{25}Mg$ and $\delta^{26}Mg$ are correlated, with a correlation coefficient of 0.754. There are two ways to normalize data for evaporation residues to those in the starting material, represented by sample R-13: (1) normalize to the average value for R-13 measured on the same day as the evaporation residue in question, which we refer to "locally" normalized data; and (2) normalize to the grand average of all DSM3-normalized data for R-13, which we refer to as "globally" normalized data. The data reported in Richter et al. (2007) were normalized by the first method, i.e., locally normalized. We report data normalized by both methods, but use the globally normalized data because they show less scatter on a plot of $\delta^{25}Mg'$ vs. $\delta^{26}Mg'$. The external reproducibility, based on the standard deviation of 34 measurements of R-13 relative to DSM3 over the period of the measurements reported here, was 0.17 ‰ for $\delta^{25}Mg$ and 0.30 ‰ for $\delta^{26}Mg$ (2σ standard deviation). In their Table 1, Richter et al. (2007) reported the standard error of 3 to 8 measurements on each sample solution bracketed by standards, with the measurements of each sample made on one or two days. Here, we follow the practice of Knight et al. (2009b) and compare the standard error with the external reproducibility divided by the square root of the number of analyses and report the larger of the two (usually the latter). All uncertainties are 2σ. Table 1 gives $\delta^{25}Mg$ and $\delta^{26}Mg$ normalized locally and globally to R-13, via

$$\delta^{25}Mg^{samp}_{R13} = \delta^{25}Mg^{samp}_{DSM3} + \delta^{25}Mg^{DSM3}_{R13} + 0.001 \times \delta^{25}Mg^{samp}_{DSM3} \times \delta^{25}Mg^{DSM3}_{R13} \quad (23)$$

and similarly for $\delta^{26}Mg^{samp}_{R13}$ (after Eq. 3 of Young and Galy, 2004). Note that the $\delta^{25}Mg^{samp}_{R13}$ values are slightly different from the values in Table 1 of Richter et al. (2007), because the last term of Eq. 23 was not taken into account in that work. The effect is small, in that the data of Richter et al. (2007) are lower by 0 to 0.09 ‰, and does not affect the conclusions of that work.

The magnesium isotopic data for CAI evaporation residues are shown in Fig. 3, a plot of $\delta^{25}Mg'$ vs. $\delta^{26}Mg'$. The locally and globally normalized data are indistinguishable on this plot, but it can be seen that the data plot close to the Rayleigh and exponential fractionation lines and

are discernibly off the power, equilibrium, and linear fractionation lines. A weighted regression (IsoPlot Model 1, Ludwig, 2003) of the locally normalized data give a value of β of 0.51332±0.00058 (2σ) with MSWD (mean square weighted deviation) = 1.09; globally normalized data gives β = 0.51279±0.00058 with MSWD = 0.48. The comparison with fractionation laws is easier to see in Fig. 4, a plot of the difference between the measured δ^{26}Mg and that calculated from δ^{25}Mg using the exponential law vs. δ^{25}Mg. The globally normalized data show significantly less scatter than the locally normalized data and are plotted in Fig. 4. We will henceforth discuss only the globally normalized data. The reason that the uncertainties in the slopes calculated from IsoPlot are the same for the globally and locally normalized data, is that they are dominated by the uncertainties in the individual data points, not the scatter in those data points. This difference is clear in the MSWD values. The globally normalized data are clearly superior and the low MSWD suggests that uncertainties on individual data points are likely overestimated. We also tried an orthogonal distance regression of both data sets, which minimizes the distance of each point orthogonal to the regression line, but does not assume any uncertainty in the individual data points, nor does it weight them. Using this approach, the locally and globally normalized data give β values of 0.51343±0.00034 and 0.51288±0.00022, respectively, which reflect the increased scatter of the locally normalized data. We adopt the IsoPlot Model 1 weighted regression of the globally normalized data, β = 0.51279±0.00058.

The slope for the evaporation experiments based on globally normalized data, 0.51279±0.00058, is slightly lower than the value based on preliminary data, 0.51400±0.00024 (Davis et al., 2005) and the value predicted from the Richter et al. (2007) experiments, above, 0.51420. The uncertainty is also somewhat larger, because Davis et al. (2005) based their uncertainties on reproducibility of each sample rather than the overall external reproducibility. The experimentally determined slope is intermediate between those predicted by the exponential (0.51101) fractionation laws and the ideal Rayleigh (0.51600) fractionation law and is significantly different from that predicted by equilibrium mass fractionation (0.52100) (Fig. 4). In terms of the generalized power law, the best-fit value for the parameter n in Eq. 22 is –0.178 ±0.058, calculated for the globally normalized data, is between the values for the exponential (approaching 0) and the ideal Rayleigh laws (–0.5) and is significantly different from the value for the equilibrium law (–1).

Richter et al. (2007) showed that α_{ij} values are temperature dependent, so by using the parameterization in Eq. 21, we would expect that β values are also temperature dependent. We calculated weighted regressions of δ^{25}Mg´ vs. δ^{26}Mg´ for evaporation experiments at each temperature from 1600 to 1900°C. All agree within error, but are permissive of a temperature effect. In order to be sure of a measurable temperature effect, higher precision isotopic analyses or experiments covering a greater range of temperatures are needed. If β values are temperature dependent, this adds uncertainty to correction for mass fractionation of data for ^{26}Al-^{26}Mg dating, because one cannot be sure of evaporation temperatures in nature. We expect that normal CAIs evaporate somewhere near the liquidus temperature of ~1400°C, but FUN inclusions with forsterite-rich initial compositions could evaporate at 1800–1900°C (Mendybaev et al., 2013). We

return to this issue later when we compare magnesium isotopic data of FUN evaporation experiments of Mendybaev et al. (2013).

Since publication of the preliminary data of Davis et al. (2005), several laboratories have adopted a power law with an exponent of 0.514. The final measured value given in this work is close to this value, but more accurate, as it is based on additional data. We recommend that magnesium isotopic compositions in CAIs and other extraterrestrial materials where evaporative mass fractionation has played a role to be corrected using $\beta = 0.5128$. We caution that there could be an evaporation temperature dependence of this β value, but the current data are not sufficiently precise to determine the temperature effect.

5. TESTS OF MASS FRACTIONATION LAWS FOR MAGNESIUM

It is rather difficult to find a natural example with which to rigorously test mass fractionation laws for magnesium. Most phases in CAIs have nonzero Al/Mg ratios, so differences in mass fractionation laws can be confused by the presence of radiogenic ^{26}Mg.

Fortunately there is one CAI that is appropriate for this test, the unusual forsterite-rich CAI Vigarano 1623-5, which is a FUN inclusion (Davis et al., 1991; Loss et al., 1994). Vigarano 1623-5 has a bulk δ^{25}Mg of 30.0 ± 1.3 ‰ (Loss et al., 1994) and abundant forsterite; the forsterite has a ^{27}Al/^{24}Mg ratio of 0.0011 (Davis et al., 1991). If this CAI had the canonical ^{26}Al/^{27}Al ratio of 5.2×10^{-5} (Jacobsen et al., 2008), this would have been sufficient to raise the δ^{26}Mg value of forsterite by a completely negligible 0.0004 ‰ (=0.4 ppm) following forsterite crystallization. The bulk composition of Vigarano 1623-5 has a ^{27}Al/^{24}Mg ratio of 0.128. Even if the CAI initially had the canonical early solar system ^{26}Al/^{27}Al and crystallized after decay of ^{26}Al, rehomogenizing its magnesium isotopic composition, forsterite would still have a δ^{26}Mg value increased by only 0.047 ‰. Thus, because of the high mass fractionation due to evaporative loss of magnesium and the relative insignificance of radiogenic ^{26}Mg in the forsterite, this CAI provides a rare opportunity to test the mass dependence of the natural "experiment" of evaporation in the solar nebula.

McKeegan et al. (2005) measured the magnesium isotopic compositions of forsterite and other phases in Vigarano 1623-5 by MC-SIMS using the UCLA Cameca ims-1270 ion microprobe with terrestrial olivine, pyroxene and spinel used as standards. The degree of magnesium isotopic mass fractionation exhibits a significant spread from one forsterite grain to another, likely because the CAI started crystallizing while it was still evaporating, a property of many FUN CAIs (Krot et al., 2008, 2010, 2014). A regression (IsoPlot Model 1, Ludwig, 2003) through only the forsterite data gives a slope of 0.5125±0.0094 and an intercept of –0.105±0.900 ‰ (2σ; MSWD = 0.14) on a plot of δ^{25}Mg´ vs. δ^{26}Mg´ (Fig. 3). The low value for MSWD for this fit indicates that uncertainties are overestimated. This is not surprising, given that uncertainties in δ^{25}Mg and δ^{26}Mg are correlated. An orthogonal distance regression without weighting the data (corresponding to IsoPlot Model 2, Ludwig, 2003) gives a slope of 0.5121±0.0036 and an intercept of –0.080±0.360 ‰ (2σ). The value of β inferred from Vigarano 1623-5 forsterite is within uncertainty of the measured value, 0.51279±0.00058, but it is also within error of the exponential law value of 0.51101. Although the data of McKeegan et al. (2005) have typical 2σ uncertainties

of 0.18, 0.33, and 0.18 ‰ for δ^{25}Mg, δ^{26}Mg, and δ^{26}Mg*, respectively, higher precision will be necessary to distinguish between the exponential law and the $\beta = 0.5128$ law.

Olsen et al. (2013) measured the magnesium isotopic composition of chondrules from the Hammadah al Hamra CB chondrite and found variations in μ^{25}Mg covering a range of about 400 ppm. These variations correlate with Al/Mg ratio, consistent with volatility fractionation. Since this meteorite formed relatively late in solar nebular history, nearly 5 Ma after CAI formation, Olsen et al. (2013) showed that little variation in μ^{26}Mg* from decay of ^{26}Al should occur over the range of Al/Mg ratios they measured. They corrected their data using the exponential law and found a correlation between μ^{26}Mg* and μ^{25}Mg, which they attributed to application of an inappropriate mass fractionation law to volatility fractionated materials. They found that the variation in μ^{26}Mg* was minimized with an exponential law with $\beta = 0.5142$, which is very close to the preliminary value of 0.514 reported by Davis et al. (2005); their data would also fit well with $\beta = 0.5128$ that we report here.

There is another set of evaporation experiments to compare with. Mendybaev et al. (2013) evaporated a series of forsterite-rich compositions with the goal of simulating the chemical and oxygen, magnesium, and silicon isotopic compositions of two FUN CAIs with large natural mass fractionation effects, Allende C1, and Vigarano 1623-5. They evaporated two compositions, FUN1, which when evaporated results in chemical composition and magnesium and silicon isotopic compositions close to those of 1623-5, and FUN2, an initial composition similar in chemical composition to 1623-5, which when evaporated results in chemical composition and magnesium and silicon isotopic compositions close to those of C1. These compositions are much more magnesium- and silicon-rich than the CAI compositions we report here. The high liquidus temperatures of these melts dictated that all experiments be run at 1900°C. The experiments were run in the same vacuum furnace as the CAI experiment reported here. Mendybaev et al. (2013) measured magnesium isotopic compositions by solution MC-ICPMS using the same Micromass IsoProbe instrument used for the data reported here, but after the instrument had been moved from the Field Museum to the University of Chicago. They also reported data collected by laser ablation MC-ICPMS using a Thermo Scientific Neptune instrument at the University of Arizona. We normalized their solution ICPMS data to their starting composition for plotting in Fig. 4. The FUN data give a slope in near perfect agreement with the CAI experiments, giving $\beta = 0.51276 \pm 0.00064$. Their laser ablation data have larger uncertainties and give $\beta = 0.51177 \pm 0.00333$, which are in agreement with the other experimental data, but also permissive of the exponential law (Fig. 4).

6. MASS-FRACTIONATION LAWS AND THE ^{26}Al-^{26}Mg SYSTEM

We have shown that evaporation of CAI-like and forsterite-rich melts produces residues that display a mass-fractionation law for magnesium that is different from any of the laws commonly used to correct data for mass fractionation. We now explore the effects of using the $\beta = 0.5128$ fractionation law on some notable ^{26}Al-^{26}Mg isochron data published over the last few years. The key fact is that the mass-fractionation correction depends only on the degree of mass fractionation, δ^{25}Mg, not on the ^{27}Al/^{24}Mg ratio. Most igneous CAIs have uniformly heavy δ^{25}Mg in all

phases in their interiors and δ^{25}Mg values approaching 0 within ~100 μm of their rims (Fahey et al., 1987b; Simon et al., 2005; Knight et al., 2009a; Bullock et al., 2013), so their bulk compositions are dominated by the interior. Thus, the choice of mass fractionation laws affects the δ^{26}Mg* value of all phases within a single CAI by a similar amount. The end result is that when data from minerals from a single CAI are plotted on an isochron diagram with δ^{26}Mg* vs. ^{27}Al/^{24}Mg, changing the fractionation law changes the intercept of an internal isochron, but not the slope. The intercepts of internal isochrons have taken on increasing importance now that analytical techniques allow enough precision to measure the 0.038 ‰ evolution of δ^{26}Mg from the initial solar system value to the present day value (Villeneuve et al., 2009; Jacobsen et al., 2008; Larsen et al., 2011), although there are disagreements on the interpretation of small differences in δ^{26}Mg among solar system materials. On the other hand, several recent investigations (Galy et al., 2004; Bizzarro et al., 2004, 2005; Young et al., 2005; Thrane et al., 2006; Jacobsen et al., 2008; Larsen et al., 2011) have studied isochrons based on analyses of bulk CAIs. In this case, the choice of fractionation law can move individual data points up or down on an isochron diagram depending on their specific δ^{25}Mg values. In principle, this will change both the slope and intercept, but the degree to which it will affect the isochron and the goodness-of-fit of the data to a single isochron will depend on the magnitude of the fractionation differences amongst individual CAIs and the fractionation law used.

The equation governing the ^{26}Al-^{26}Mg system is

$$\left(\frac{^{26}\mathrm{Mg}}{^{24}\mathrm{Mg}}\right)=\left(\frac{^{26}\mathrm{Mg}}{^{24}\mathrm{Mg}}\right)_0+\left(\frac{^{27}\mathrm{Al}}{^{24}\mathrm{Mg}}\right)\left(\frac{^{26}\mathrm{Al}}{^{27}\mathrm{Al}}\right)_0, \quad (24)$$

where ^{26}Mg/^{24}Mg is the ratio measured today, (^{26}Mg/^{24}Mg)$_0$ is the initial ratio established at the last time the object was isotopically homogenized, ^{27}Al/^{24}Mg is the ratio measured today, and (^{26}Al/^{27}Al)$_0$ was the ratio at the last time the object was homogenized. Data are plotted in an isochron diagram of ^{26}Mg/^{24}Mg vs. ^{27}Al/^{24}Mg. If the system is well-behaved, a regression line is fit to the data and (^{26}Mg/^{24}Mg)$_0$ is the intercept and (^{26}Al/^{27}Al)$_0$ is the slope. Mass-dependent fractionation of magnesium can affect ^{26}Mg/^{24}Mg and (^{26}Mg/^{24}Mg)$_0$, so it is necessary to correct each measured ^{26}Mg/^{24}Mg by normalizing the corresponding measured ^{25}Mg/^{24}Mg ratio to the chondritic ^{25}Mg/^{24}Mg ratio of 0.12663 (Catanzaro et al., 1966; or to the more precise recently measured value of Bizzarro et al., 2011, 0.126896±0.000025) and using a mass-fractionation law to relate fractionation in ^{26}Mg/^{24}Mg to that in ^{25}Mg/^{24}Mg. This gives unfractionated ratios, (^{26}Mg/^{24}Mg)$_{uf}$ and changes the governing equation to:

$$\left(\frac{^{26}\mathrm{Mg}}{^{24}\mathrm{Mg}}\right)_{uf}=\left(\frac{^{26}\mathrm{Mg}}{^{24}\mathrm{Mg}}\right)_{uf,0}+\left(\frac{^{27}\mathrm{Al}}{^{24}\mathrm{Mg}}\right)\left(\frac{^{26}\mathrm{Al}}{^{27}\mathrm{Al}}\right)_0. \quad (25)$$

(^{26}Mg/^{24}Mg)$_{uf}$ can also be expressed in terms of the δ^{26}Mg* value, using

$$\left(\frac{^{26}\mathrm{Mg}}{^{24}\mathrm{Mg}}\right)_{uf}=\left(\frac{\delta^{26}\mathrm{Mg}^*}{1000}+1\right)\times\left(\frac{^{26}\mathrm{Mg}}{^{24}\mathrm{Mg}}\right)_{uf,0}. \quad (26)$$

In calculating $\delta^{26}Mg^*$, it is tempting to simply use δ' values in place of δ values (as is done by Young et al., 2005, and Wasserburg et al., 2012), as they are easily corrected for fractionation using exponential-type fractionation laws, but

$$\delta^{26}Mg^* = \delta^{26}Mg'_{meas} - \frac{\delta^{25}Mg'_{meas}}{\beta} \quad (27)$$

can give significantly incorrect values for $\delta^{26}Mg^*$. It is necessary to convert δ values to δ' values, make the fractionation correction, convert back to δ values, and then calculate $\delta^{26}Mg^*$ using $\delta^{26}Mg^* = \delta^{26}Mg_{meas} - \delta^{26}Mg_{corr}$. Using the exponential correction methods, this can be expressed as:

$$\delta^{26}Mg^* = \delta^{26}Mg_{meas} - \left[\left(1+\frac{\delta^{25}Mg_{meas}}{1000}\right)^{\frac{1}{\beta}} - 1\right] \times 1000, \quad (28)$$

where we recommend using β=0.5128.

Use of Eq. 27 gives lower or higher $\delta^{26}Mg^*$ values than Eq. 28, depending primarily on the magnitude of $\delta^{25}Mg$ and the sign and magnitude of $\delta^{26}Mg^*$, and there is only a slight dependence on β; for positive $\delta^{26}Mg^*$, Eq. 27 gives lower $\delta^{26}Mg^*$ values than Eq. 28. Eq. 27 can give values that are incorrect by amounts that are much larger than current analytical uncertainties.

7. IMPLICATIONS FOR ^{26}Al IN THE SOLAR SYSTEM

The first hint that CAIs formed with an initial $^{26}Al/^{27}Al$ ratio significantly above the canonical value of ~5×10^{-5} (MacPherson et al., 1995) was a model isochron, a line between the bulk composition of an Allende CAI and normal isotopic composition, which gave $(^{26}Al/^{27}Al)_0$ = $(6.24\pm0.23)\times10^{-5}$ (Galy et al., 2000). Those authors used a linear fractionation correction, Eq. 12, with θ = 0.5163. Correcting their data using the β = 0.5128 law in Eq. 28 gives $(^{26}Al/^{27}Al)_0$ = $(5.91\pm0.22)\times10^{-5}$, ~5 % lower than the value they reported, but still higher than the 'canonical' value of $(5.23\pm0.13)\times10^{-5}$ reported by Jacobsen et al. (2008).

Young et al. (2005) presented solution measurements on three whole rock CAIs and laser ablation MC-ICPMS data for about 300 spots on eight CAIs from CV chondrites. The three whole rock samples define an apparent isochron with a slope corresponding to $(^{26}Al/^{27}Al)_0$ = $(7.0\pm1.3)\times10^{-5}$ and an intercept of $\delta^{26}Mg_0 = -0.1\pm0.2$ ‰. They also found that many of the spot analyses plotted to the ^{26}Mg-rich side of the canonical $(^{26}Al/^{27}Al)_0$ isochron at ~5×10^{-5} and coined the term "supracanonical" to describe the higher inferred $^{26}Al/^{27}Al$ ratios. This initiated a debate that persisted for several years about whether supracanonical $^{26}Al/^{27}Al$ ratios were real. Young et al. (2005) used Eq. 27 with β = 0.521 (the value for equilibrium fractionation) to correct their data for mass fractionation. Using Eq. 28 rather than Eq. 27 to correct for mass fractionation with β = 0.521, the inferred $(^{26}Al/^{27}Al)_0$ increases to $(7.1\pm1.3)\times10^{-5}$ and using β =

607 0.5128 rather than $\beta = 0.521$ lowers it to $(6.5\pm1.3)\times10^{-5}$. The laser ablation spots on eight CAIs
608 show a range of isotopic composition, with inferred $(^{26}Al/^{27}Al)_0$ as high as 7.0×10^{-5}, however
609 with use of Eq. 27 and $\beta = 0.521$, all the laser ablation data yield $(^{26}Al/^{27}Al)_0 = (5.56\pm0.13)\times10^{-5}$.
610 If Eq. 28 is used instead of Eq. 27 to correct for mass fractionation with $\beta = 0.521$, the inferred
611 $(^{26}Al/^{27}Al)_0$ increases to $(5.63\pm0.13)\times10^{-5}$ but using $\beta = 0.5128$ rather than $\beta = 0.521$ lowers it to
612 $(5.46\pm0.13)\times10^{-5}$. The effect of using the correct fractionation correction equation is to slightly
613 increase inferred $(^{26}Al/^{27}Al)_0$ ratios, and use of the experimentally derived β value for CAI evap-
614 oration lowers the ratios, but not by enough to make the apparent supracanonical $(^{26}Al/^{27}Al)_0$ ra-
615 tios become canonical (all errors are 2σ).

616 Bizzarro et al. (2004) reported a slope corresponding to $(^{26}Al/^{27}Al)_0 = (5.25\pm0.10) \times10^{-5}$
617 based on MC-ICPMS measurements of large chips of CAIs and amoeboid olivine aggregates
618 (AOAs). Bizzarro et al. (2005) published revised $^{27}Al/^{24}Mg$ ratios for these samples, because of a
619 computational error, which led to a revised slope corresponding to $(^{26}Al/^{27}Al)_0 = (5.83\pm0.11)$
620 $\times10^{-5}$. Thrane et al. (2006) reported data on additional CAIs and combined their data with
621 Bizzarro et al. (2004, 2005) to provide a very precise slope corresponding to $(^{26}Al/^{27}Al)_0 =$
622 $(5.85\pm0.05) \times10^{-5}$, which appeared to confirm supracanonical $^{26}Al/^{27}Al$ ratios. All of these data
623 were corrected for mass fractionation by using the exponential law. Subsequent isochrons based
624 on several bulk CAIs by Jacobsen et al. (2008) and Larsen et al. (2011) give lower $(^{26}Al/^{27}Al)_0$
625 values, making it likely that the earlier data of Bizzarro et al. (2004, 2005) and Thrane et al.
626 (2006) are incorrect, most likely in the Al/Mg ratios, so we will not attempt to address the effects
627 of fractionation law corrections for those earlier works.

628 Jacobsen et al. (2008) measured magnesium isotopic compositions and Al/Mg ratios on six
629 whole-rock CAIs and three microdrilled CAI samples, all from the Allende CV3 chondrite. They
630 reported an isochron slope corresponding to $(^{26}Al/^{27}Al)_0 = (5.23\pm0.13)\times10^{-5}$ with $\delta^{26}Mg_0 =$
631 -0.040 ± 0.029 ‰, using an exponential law with $\beta = 0.511$, and recommended this as the early
632 solar system $(^{26}Al/^{27}Al)_0$ value. They also separated minerals from three of the CAIs and com-
633 bined the mineral-separate and whole-rock data to evaluate the effect of different values of β for
634 exponential fractionation laws. They found that using the exponential ($\beta = 0.511$), experimental
635 ($\beta = 0.514$), and equilibrium ($\beta = 0.521$) values gave $(^{26}Al/^{27}Al)_0$ values of $(5.11\pm0.14)\times10^{-5}$,
636 $(5.18\pm0.20)\times10^{-5}$, and $(5.31\pm0.35)\times10^{-5}$, respectively. They argued that since the exponential
637 law gave the most precise fit, it must be correct (i.e., best reproduced isotopic fractionation of
638 natural samples). However, just because the slope derived is more precise with an exponential
639 law is not sufficient evidence to conclude that the exponential value must be correct. There are
640 still relatively few data points and there could be a real spread in the timing of Al/Mg fractiona-
641 tion of whole CAIs. Furthermore, data on mineral separates and whole rocks are combined but
642 these can be dating different events. For example, whole rock values can record the time of ma-
643 jor Al/Mg fractionation of bulk CAIs or their progenitors, whereas mineral separates or individu-

al mineral analyses can record the time of last melting. Recent high-precision data on Vigarano CAIs indicates that these times are not the same: the evidence suggests that the major Al/Mg fractionation event that led to evaporative mass fractionation of most normal CAIs occurred approximately at the time of canonical $(^{26}Al/^{27}Al)_0 = 5.2\times10^{-5}$, whereas melting and crystallization events affecting individual CAIs began at this time, but continued for ~0.7 Ma (MacPherson et al., 2012). In a supplement to their paper, Jacobsen et al. (2008) evaluated the effect of changing β on the whole-rock CAI data alone. For $\beta = 0.511$, 0.514, and 0.521, they found $(^{26}Al/^{27}Al)_0$ ratios of $(5.23\pm0.14)\times10^{-5}$, $(5.19\pm0.12)\times10^{-5}$, and $(4.81\pm0.30)\times10^{-5}$, with initial magnesium isotopic compositions, $\delta^{26}Mg_0$, of –0.040±0.029, –0.001±0.031, and 0.156±0.087 ‰, respectively. Here, the preliminary experimentally determined value of $\beta = 0.514$ (Davis et al., 2005) gives the most precise slope and $\beta = 0.511$ and $\beta = 0.514$ give intercepts within error of the initial magnesium isotopic composition calculated from the present day terrestrial value, $\delta^{26}Mg = 0$, and $(^{26}Al/^{27}Al)_0 = (5.19\pm0.12)\times10^{-5}$: $\delta^{26}Mg_0 = –0.038\pm0.001$ ‰. Unfortunately, none of the tests Jacobsen et al. did with different fractionation laws can be reevaluated here, because their data table contains only $^{27}Al/^{24}Mg$ and $\delta^{26}Mg^*$; $\delta^{25}Mg$ and $\delta^{26}Mg$ are also needed to test fractionation laws. Jacobsen et al. (2008) used Eq. 28 to correct for mass fractionation.

Wasserburg et al. (2012) studied ^{26}Al-^{26}Mg systematics by solution MC-ICPMS in several physically separated fractions of the Allende CAI Egg-3, for which a ^{26}Al-^{26}Mg isochron with an intercept of $\delta^{26}Mg_0 = \sim–1$ ‰ was reported by Esat et al. (1980). They found that the intercept was still negative, but smaller: $\delta^{26}Mg_0 = \sim–0.127\pm0.032$ ‰. They also evaluated the effect of mass fractionation laws on the goodness of fit of the Egg-3 isochron with a plot of MSWD vs. β. Wasserburg et al. (2012) write that they reduced the data for Egg-3 using the exponential law ($\beta = 0.511$). Careful comparison of their $\delta^{25}Mg$, $\delta^{26}Mg$, and $\delta^{26}Mg^*$ data shows that they used Eq. 27 rather than Eq. 28. For Egg-3, they found that the minimum MSWD was at $\beta = 0.511$. We recalculated $\delta^{26}Mg^*$ from their $\delta^{25}Mg$ and $\delta^{26}Mg$ values using Eq. 28 and found that the minimum MSWD remained at $\beta = 0.511$. Wasserburg et al. also discarded one of their data points as an outlier, although there was no reason offered for discarding the data point beyond it being an outlier. If this data point is included, the minimum MSWD moved to $\beta = 0.516$, a significant shift, where the intercept of the isochron changes to $\delta^{26}Mg_0 = –0.018\pm0.031$ ‰. The MSWD vs. β curves are fairly broad and certainly permissive of $\beta = 0.5128$. We consider the Egg-3 data of Wasserburg et al. (2012) to be entirely consistent with our experimentally measured β value. We were unable to reproduce Wasserburg et al.'s calculations on the data of Jacobsen et al. (2008), because $\delta^{26}Mg$ was not reported in the latter publication.

Larsen et al. (2011) reported a new isochron based on whole rock CAIs and amoeboid olivine aggregates from the Efremovka CV3 chondrite that give $(^{26}Al/^{27}Al)_0 = (5.25\pm0.02)\times10^{-5}$, in excellent agreement with Jacobsen et al. (2008), and $\delta^{26}Mg_0 = -0.0159 \pm 0.0014$ ‰, barely within uncertainty of the Jacobsen et al. value and clearly different from the expected early solar system value of –0.038 ‰ (Villeneuve et al., 2009). Larsen et al. used the exponential law, $\beta = 0.511$, to correct their data for mass fractionation. They noted that their data disagreed with that of Bizzarro et al. (2005) and Thrane et al. (2006), but did not offer an explanation of why the earlier data were incorrect.

Although the apparent agreement with Jacobsen et al. (2008) would seem to settle the question of initial $^{26}Al/^{27}Al$ ratio of the solar system, some issues arise when the Larsen et al. (2011) data are examined in detail. In their Table 1, they give values for $\mu^{25}Mg$, $\mu^{26}Mg$, and $\mu^{26}Mg^*$. A problem arises when these data are tested against fractionation laws: application of the exponential law to their $\mu^{25}Mg$ and $\mu^{26}Mg$ data calculated using Eq. 28 should match the $\mu^{26}Mg^*$ given in their data table, within uncertainties. Instead, all of these calculated $\mu^{26}Mg^*$ values are lower than the values in their data table, by 2.2 to 36 ppm, which is outside their quoted errors of 2–4 ppm. If instead, one uses the flawed Eq. 27, calculated $\mu^{26}Mg^*$ values are closer to those in the data table, but are still lower by 4–10 ppm. On the other hand, use of Eq. 18 gives $\mu^{26}Mg^*$ values that are higher than those in the data table by 4 to 172 ppm, so it is unlikely that this demonstrably incorrect equation was used by Larsen et al. (2011). One can also solve Eq. 28 for β, expressing it in terms of μ-values:

$$\beta = \frac{\ln\left(\frac{\mu^{25}Mg}{10^6}+1\right)}{\ln\left(\frac{\mu^{26}Mg-\mu^{26}Mg^*}{10^6}+1\right)}. \quad (29)$$

For the CAIs and AOAs that comprise the Larsen et al. (2011) isochron and have significant mass-fractionation effects ($\mu^{25}Mg$ >1000 ppm or $\mu^{25}Mg$ <–1000 ppm), the calculated β values range from 0.5099 to 0.5127, which is a significant range for such high precision data.

We would like to understand the effect of β values on the Larsen et al. (2011) isochron and will consider two possibilities. (1) Perhaps most likely, is that Larsen et al. (2011) do an exponential-law correction on every measured isotope ratio and report the average of these values in their Table 1. In this case, uncertainties in $\mu^{26}Mg^*$ are smaller than those in $\mu^{25}Mg$ and $\mu^{26}Mg$, because of correlated errors in the latter μ-values (as the ^{24}Mg signal is the denominator in both isotope ratios). In this case, one should ignore the reported $\mu^{26}Mg$ values and calculate new ones from $\mu^{25}Mg$ and $\mu^{26}Mg^*$ using the exponential law. If this is correct, we remain puzzled by the fact that Eq. 28 gives calculated $\mu^{26}Mg^*$ values that are consistently slightly lower than those reported in Table 1 of Larsen et al. (2011): we might expect some variation, but with some high and some lower than the reported values. (2) We disregard the reported $\mu^{26}Mg^*$ values and accept the reported $\mu^{25}Mg$ and $\mu^{26}Mg$ values and calculate new $\mu^{26}Mg^*$ values using Eq. 28 and appropriate β values. The issue here is that the uncertainties in the new $\mu^{26}Mg^*$ values will be much larger than those reported by Larsen et al. (2011) because of propagation of the larger uncertainties in $\mu^{25}Mg$ and $\mu^{26}Mg$.

We used IsoPlot (Ludwig, 2003) to fit isochrons. IsoPlot Model 1 is a regression that weights each point by its uncertainty in $^{27}Al/^{24}Al$ and $\mu^{26}Mg^*$ and reports the Mean Square Weighted Deviation (MSWD). When MSWD is statistically significantly above 1, IsoPlot recommends using Model 2, which does not weight the individual points, but minimizes the distance of each point orthogonal to the regression line. Using the $^{27}Al/^{24}Al$ and $\mu^{26}Mg^*$ data in Table 1 of Larsen et al. (2011) and IsoPlot Model 1, we calculate a slope corresponding to $(^{26}Al/^{27}Al)_0 = (5.253\pm0.018)\times10^{-5}$ and an intercept of $\mu^{26}Mg_0 = -16.0\pm1.2$ ppm, with MSWD = 1.3, very close to the values in their paper. Any differences are likely due to rounding errors or a slightly different value assumed for the terrestrial $^{26}Mg/^{24}Mg$ ratio. If we ignore the reported $\mu^{26}Mg$ values and calculate new ones from $\mu^{25}Mg$ and $\mu^{26}Mg^*$ using the exponential law, then apply our $\beta = 0.5128$ fractionation law, IsoPlot Model 1 gives a slope corresponding to $(^{26}Al/^{27}Al)_0 = (5.45\pm0.18)\times10^{-5}$ and an intercept of $\mu^{26}Mg_0 = -27\pm12$ ppm, with MSWD = 66, indicating a poor fit. The reason for the deterioration in the fit compared to $\beta = 0.511$ is that some CAIs are isotopically light and others are isotopically heavy, so changes in β move $\mu^{26}Mg^*$ in opposite directions. If we ignore the reported $\mu^{26}Mg^*$ values and calculate new ones from $\mu^{25}Mg$ and $\mu^{26}Mg$ using $\beta = 0.511$, we obtain a slope corresponding to $(^{26}Al/^{27}Al)_0 = (5.277\pm0.095)\times10^{-5}$ and an intercept of $\mu^{26}Mg_0 = -8\pm14$ ppm, with MSWD = 0.51, using Model 1. The uncertainties in the slope and intercept are larger because the uncertainties in $\mu^{26}Mg^*$ are propagated from those in $\mu^{25}Mg$ and $\mu^{26}Mg$. If we recalculate $\mu^{26}Mg^*$ from $\mu^{25}Mg$ and $\mu^{26}Mg$ using our $\beta = 0.5128$ fractionation law, IsoPlot Model 1 gives a slope corresponding to $(^{26}Al/^{27}Al)_0 = (5.50\pm0.22)\times10^{-5}$ and an intercept of $\mu^{26}Mg_0 = -18\pm46$ ppm, with MSWD = 7.9, again indicating a poor fit. The bottom line is that the values in Table 1 of Larsen et al. (2011) for $^{27}Al/^{24}Al$ and $\mu^{26}Mg^*$ are very sensitive to the fractionation law and values other than $\beta = 0.511$ cause the CAI data points to scatter. If $\beta = 0.5128$, as expected for evaporative mass fractionation of magnesium, these CAIs are not isochronous.

The Larsen et al. (2011) isochron is also controversial because the intercept of their AOA-CAI isochron is at $\mu^{26}Mg_0 = -15.9\pm1.4$ ppm, whereas the intercept expected from extrapolating back from the terrestrial $\mu^{26}Mg$ value of 0 ppm using the solar system $^{27}Al/^{24}Mg$ ratio and a $(^{26}Al/^{27}Al)_0$ ratio of 5.2×10^{-5} gives an initial $\mu^{26}Mg_0$ value of –38 ppm. Larsen et al. (2011) attributed this difference to solar nebular heterogeneity of $(^{26}Al/^{27}Al)_0$ or $\mu^{26}Mg_0$ or both. Wasserburg et al. (2012) questioned whether AOAs should be included in the isochron and recalculated an isochron using the CAI data alone in Larsen et al. (2011), and found an intercept of $\mu^{26}Mg_0 = -30\pm40$ ppm, which is in agreement with the intercept of the Jacobsen et al. (2008) isochron (–40±29 ppm) and with the extrapolated terrestrial value of –38 ppm.

8. FUN CAIS

Among FUN CAIs, Allende EK1-4-1 and C1 have reported $\delta^{26}Mg^*$ values of ~–3.7 and ~–1.8 ‰, respectively. C1 was measured several times (Lee and Papanastassiou, 1974; Lee et al., 1976; Wasserburg et al., 1977; Esat et al., 1978) and consistently gave negative $\delta^{26}Mg^*$, howev-

er all the data were corrected for mass fractionation using the '70s Caltech law ($\beta = 0.500$). The methodology was established by Lee and Papanastassiou (1974) who explicitly describe this law for fractionation correction. When the 1970s Caltech data are reprocessed according to our recommended fractionation law ($\beta = 0.5128$), EK1-4-1 is left with a smaller $\delta^{26}Mg^*$ anomaly (–2.8 ‰) and the one for C1 is only –0.2±0.3 ‰. The Vigarano FUN CAI 1623-5 is an isotopic twin of C1. Our ion microprobe data for 1623-5 suggest a slight positive $\delta^{26}Mg^*$ when corrected for mass fractionation with either our recommended fractionation law, $\beta = 0.5128$, or the exponential law, $\beta = 0.5110$ (Fig. 4) and the anomaly in Allende C1 is not resolved with the precision of the 1970s Caltech data. Thus, the only CAIs with unambiguous negative $\delta^{26}Mg^*$ anomalies are EK1-4-1 (Wasserburg et al., 1977) and a few hibonite crystals from CM chondrites (Liu et al., 2009).

8. CONCLUSIONS

It is now clear that in the new era of high precision magnesium isotopic analysis by multicollector methods, it is essential to give data on measured $\delta^{25}Mg$ and $\delta^{26}Mg$ and inferred $\delta^{26}Mg^*$, to explain how uncertainties in data are obtained and what standards are used, and to state what fractionation law is used to correct data for natural isotopic mass fractionation. When comparing data between different laboratories, it is highly desirable to use the same mass-fractionation law. This will reduce the potential for disagreements over key issues such as the value and spatial homogeneity of the initial $^{26}Al/^{24}Mg$ of the solar system that arise from different definitions of the parameters necessary to derive a slope on the Al-Mg evolution diagram. Since the most likely cause of the large mass-fractionation effects in CAIs is evaporation, we recommend that data be corrected with Eq. 28 by using an exponent of $\beta = 0.5128$. We caution against overinterpretation of very small differences in apparent initial $\delta^{26}Mg^*$ values of various refractory phases in meteorites as indicative of large-scale heterogeneities in $^{26}Al/^{27}Al$ in the solar nebula for several reasons: (1) the fractionation law that applies to high-temperature evaporation of silicates may be temperature dependent and the evaporation temperature in nature is not known; (2) there are heterogeneities in the early solar system $\delta^{26}Mg_0$ values for a few CAIs (EK1-4-1 and a few hibonite CAIs) that are currently unexplained. The most robust constraints on solar system chronology in high-temperature events in the nebula are still best derived from refractory parent-daughter fractionations and not model evolution curves of less-refractory daughter elements.

ACKNOWLEDGEMENTS

We thank Ian D. Hutcheon for providing the data plotted in the Galy et al. (2004) abstract, Martin Bizzarro for information on fractionation corrections used by Bizzarro et al. (2004), Levke Kööp for a careful reading of the manuscript, and Gary Huss and Benjamin Jacobsen for thorough and constructive reviews of this paper. This work was supported by the National Aeronautics and Space Administration through grant NNX09AG39G (AMD), NNX09AG38G (FMR), NNX07AH14G (MW), and NNH08ZDA001N (KDM). The UCLA ion microprobe laboratory is partially supported by a grant from the NSF Instrumentation and Facilities program.

REFERENCES

Albarède F. and Beard B. (2004) Analytical methods for non-traditional isotopes. *Rev. Mineral. Geochem.* **55**, 113–152.

Albarède F., Telouk P., Blichert-Toft J., Boyet M., Agranier A. and Nelson B. (2004) Precise and accurate isotopic measurements using multiple-collector ICPMS. *Geochim. Cosmochim. Acta* **68**, 2725–2744.

Andrén H., Rodushkin I., Steinberg A, Malinovsky D. and Baxter D. C. (2004) Sources of mass bias and isotope ratio variation in multicollector ICP-MS: optimization of instrumental parameters based on experimental observations. *J. Anal. At. Spectrom.* **19**, 1217–1224.

Bizzarro M., Baker J. A. and Haack H. (2004) Mg isotope evidence for contemporaneous formation of chondrules and refractory inclusions. *Nature* **431**, 275–278.

Bizzarro M., Baker J. A. and Haack H. (2005) Corrigendum: Mg isotope evidence for contemporaneous formation of chondrules and refractory inclusions. *Nature* **435**, 1280.

Bizzarro M., Paton C., Larsen K., Schiller M., Trinquier A. and Ulfbeck D. (2011) High-precision Mg-isotope measurements of terrestrial and extraterrestrial material by HR-MC-ICPMS—implications for the relative and absolute Mg-isotope composition of the bulk silicate Earth. *J. Anal. At. Spectrom.* **26**, 565–577.

Bourdon B., Tipper E. T., Fitoussi C and Stracke A. (2010) Chondritic Mg isotope composition of the Earth. *Geochim. Cosmochim. Acta* **74**, 5069–5083.

Bullock E. S., Knight K. B., Richter F. M., Kita N. T., Ushikubo T., MacPherson G. J., Davis A. M. and Mendybaev R. A. (2013) Mg and Si isotopic fractionation patterns in types B1 and B2 CAIs: implications for formation under different nebular conditions. *Meteorit. Planet. Sci.* **48**, 1440–1458.

Catanzaro E. J., Murphy T. J., Garner E. L. and Shields W. R. (1966) Absolute isotopic abundance ratios and atomic weights of magnesium. *J. Res. Nat. Bur. Standards* **70a**, 453–458.

Chakrabarti R. and Jacobsen S. B. (2010) The isotopic composition of magnesium in the inner solar system. *Earth Planet. Sci. Lett.* **293**, 349–358.

Clayton R. N., MacPherson G. J., Hutcheon I. D., Davis A. M., Grossman L., Mayeda T. K., Molini-Velsko C., and Allen J. M. (1984) Two forsterite-bearing FUN inclusions in the Allende meteorite. *Geochim. Cosmochim. Acta* **48**, 535–548.

Clayton R. N., Hinton R. W. and Davis A. M. (1988) Isotopic variation in the rock-forming elements in meteorites. *Phil. Trans. R. Soc. Lond.* **A325**, 483–501.

Davis A. M. & McKeegan K. D. (2014) Short-lived radionuclides and early solar system chronology. In *Meteorites and Cosmochemical Processes* (Ed. A. M. Davis), Vol. 1 *Treatise on Geochemistry, 2nd Ed.* (Exec. Eds. H. D. Holland and K. K. Turekian), Elsevier, Oxford, pp. 361–395.

Davis A. M., Hashimoto A., Clayton R. N. and Mayeda T. K. (1990) Isotope mass fractionation during evaporation of Mg_2SiO_4. *Nature* **347**, 655–658.

Davis A. M., MacPherson G. J., Clayton R. N., Mayeda T. K., Sylvester P. J., Grossman L., Hinton R. W. and Laughlin J. R. (1991) Melt solidification and late-stage evaporation in the evolution of a FUN inclusion from the Vigarano C3V chondrite. *Geochim. Cosmochim. Acta* **55**, 621–637.

Davis A. M., Richter F. M., Mendybaev R. A., Janney P. E., Wadhwa M. and McKeegan K. D. (2005) Isotopic mass fractionation laws and the initial solar system $^{26}Al/^{27}Al$ ratio. *Lunar Planet. Sci.* **36** #2334.

Esat M. T. (1984) A 61 cm radius multi-detector mass spectrometer at the Australian National University. *Nucl. Instrum. Meth. Phys. Res.* **B5**, 545–553.

Esat T. M., Lee T., Papanastassiou D. A. and Wasserburg G. J. (1978) Search for ^{26}Al effects in the Allende FUN inclusion C1. *Geophys. Res. Lett.* **5**, 807–810.

Esat T. M., Brownlee D. E., Papanastassiou D. A. and Wasserburg G. J. (1979) Magnesium isotopic composition of interplanetary dust particles. *Science* **206**, 190–197.

Esat T. M., Papanastassiou D. A., and Wasserburg G. J. (1980) The initial state of ^{26}Al and $^{26}Mg/^{24}Mg$ in the early solar system. *Lunar Planet. Sci.* **11**, 262–264.

Fahey A. J., Goswami J. N., McKeegan K. D. and Zinner E. (1987a) ^{26}Al, ^{244}Pu, ^{50}Ti, REE, and trace element abundances in hibonite grains from CM and CV meteorites. *Geochim. Cosmochim. Acta* **51**, 329–350.

Fahey A. J., Zinner E. K., Crozaz G. and Kornacki A. S. (1987b) Microdistribution of Mg isotopes and REE abundances in a Type A calcium-aluminum-rich inclusion from Efremovka. *Geochim. Cosmochim. Acta* **51**, 3215–3229.

Galy A., Young E. D., Ash R. D. and O'Nions R. K. (2000) The formation of chondrules at high gas pressures in the solar nebula. *Science* **290**, 1751–1753.

Galy A., Yoffe O., Janney P. E., Williams R. D., Cloquet C., Alard O., Halicz L., Wadhwa M., Hutcheon I. D., Ramon E. and Carignan J. (2003) Magnesium isotope heterogeneity of the isotopic standard SRM980 and new reference materials for magnesium-isotope-ratio measurements. *J. Anal. At. Spectrom.* **18**, 1352–1356.

Galy A., Hutcheon I. D. and Grossman L. (2004) $(^{26}Al/^{27}Al)_0$ of the solar nebula inferred from Al-Mg systematic in bulk CAIs from CV3 chondrites. *Lunar Planet. Sci.* **25**, #1790.

Grossman L., Ebel D. S., Simon S. B., Davis A. M., Richter F. M. and Parsad N. M. (2000) Major element chemical and isotopic compositions of refractory inclusions in C3 chondrites: the separate roles of condensation and evaporation. *Geochim. Cosmochim. Acta* **64**, 2879–2894.

Grossman L., Ebel D. S. and Simon S. B. (2002) Formation of refractory inclusions by evaporation of condensate precursors. *Geochim. Cosmochim. Acta* **68**, 145–161.

Grossman L., Simon S. B., Rai V. K., Thiemens M. H., Hutcheon I. D., Williams R. W., Galy A., Ding T., Fedkin A. V., Clayton R. N. and Mayeda T. K. (2008) Primordial compositions of refractory inclusions. *Geochim. Cosmochim. Acta* **72**, 3001–3021.

Habfast K. (1998) Fractionation correction and multiple collectors in thermal ionization isotope ratio mass spectrometry. *Int. J. Mass Spectrom.* **176**, 133–148.

Handler M. R., Baker J. A., Schiller M., Bennett V. C. and Yaxley G. M. (2009) Magnesium stable isotope composition of the Earth's upper mantle. *Earth Planet. Sci. Lett.* **282**, 306–313.

Hart S. R. and Zindler A. (1989) Isotopic fractionation laws: a test using calcium. *Int. J. Mass Spectrom. Ion Proc.* **89**, 287–301.

Hulston J. R. and Thode H. G. (1965) Variations in the S^{33}, S^{34}, and S^{36} contents of meteorites and their relation to chemical and nuclear effects. *J. Geophys. Res.* **70**, 3475–3484.

Hutcheon I. D. (1982) Ion probe magnesium isotopic measurements of Allende inclusions. *Amer. Chem. Soc. Symp. Ser.* **176**, 95–128.

Ireland T. R., Fahey A. J. and Zinner E. K. (1991) Hibonite bearing microspherules—a new type of refractory inclusions with large isotopic anomalies. *Geochim. Cosmochim. Acta* **55**, 367–379.

Jacobsen B., Yin Q.-Z., Moynier F., Amelin Y., Krot A. N., Nagashima K., Hutcheon I. D. and Palme H. (2008) ^{26}Al-^{26}Mg and ^{207}Pb-^{206}Pb systematics of Allende CAIs: canonical solar initial ^{26}Al/^{27}Al ratio reinstated. *Earth Planet. Sci. Lett.* **272**, 353–364.

Kita N. T., Ushikubo T., Knight K. B., Mendybaev R. A., Davis A. M., Richter F. M. and Fournelle J. H. (2012) Internal ^{26}Al-^{26}Mg isotope systematics of a Type B CAI: remelting of refractory precursor solids. *Geochim. Cosmochim. Acta* **86**, 37–51.

Knight K. B., Kita N. T., Davis A. M., Richter F. M. and Mendybaev R. A. (2009a) Mg and Si isotope fractionation within three Type B Ca-Al-rich inclusions. *Lunar Planet. Sci.* **40**, #2360.

Knight K. B., Kita N. T., Mendybaev R. A., Richter F. M., Davis A. M. and Valley J. W. (2009b) Silicon isotopic fractionation of CAI-like vacuum evaporation residues. *Geochim. Cosmochim. Acta* **73**, 6390–6401.

Krot A. N., Nagashima K., Hutcheon I. D., Davis A. M., Thrane K., Bizzarro M., Huss G. R., Papanastassiou D. A. and Wasserburg G. J. (2008) Oxygen isotopic compositions of individual minerals from FUN CAIs. *Lunar Planet. Sci.* **39**, #2162.

Krot A. N., Nagashima K., Ciesla F. J., Meyer B. S., Hutcheon I. D., Davis A. M., Huss G. R. and Scott E. R. D. (2010) Oxygen isotopic composition of the Sun and mean oxygen isotopic composition of the protosolar silicate dust: evidence from refractory inclusions. *Astrophys. J.* **713**, 1159–1166.

Krot A. N., Nagashima K., Wasserburg G. J., Huss G. R., Papanastassiou D., Davis A. M., Hutcheon I. D., and Bizzarro M. (2014) Calcium-aluminum-rich inclusions with fractionation and unknown nuclear effects (FUN CAIs): I. Mineralogy, petrology, and oxygen isotopic compositions. *Geochim. Cosmochim. Acta* **145**, 206–247.

Larsen K., Trinquier A., Paton C., Schiller M., Wielandt D., Ivanova M. A., Connelly J. N., Nordlund Å., Krot A. N. and Bizzarro M. (2011) Evidence for magnesium isotope heterogeneity in the solar protoplanetary disk. *Astrophys. J.* **735**, L37 (7 pp).

Lee T. and Papanastassiou D. A. (1974) Mg isotopic anomalies in the Allende meteorite and correlation with O and Sr effects. *Geophys. Res. Lett.* **1**, 225–228.

Lee T., Papanastassiou D. A. and Wasserburg G. J. (1976) Demonstration of ^{26}Mg excess in Allende and evidence for ^{26}Al. *Geophys. Res. Lett.* **3**, 109–112.

Liu M. C., McKeegan K. D., Goswami J. N., Marhas K. K., Sahijpal S., Ireland T. R. and Davis A. M. (2009) Isotopic records in CM hibonites: Implications for timescales of mixing of isotope reservoirs in the solar nebula. *Geochim. Cosmochim. Acta* **73**, 5051–5079.

Loss R. D., Lugmair G. W., Davis A. M. and MacPherson G. J. (1994) Isotopically distinct reservoirs in the solar nebula: isotope anomalies in Vigarano meteorite *inclusions. Astrophys. J.* **436**, L193–L196.

Ludwig K. (2003) ISOPLOT: a geochronological toolkit for Microsoft Excel 3.00. Berkeley Geochronology Center Special Publication No. 4, Berkeley, CA 94709.

Lundberg L. L., Zinner E. and Crozaz G. (1994) Search for isotopic anomalies in oldhamite (CaS) from unequilibrated (E3) enstatite chondrites. *Meteoritics* **29**, 384–393.

Luu T.-H., Chaussidon M., Mishra R. K., Rollion-Bard C., Villeneuve J., Srinivasan G., and Birck J.-L. (2013) High precision Mg isotope measurements of meteoritic samples by secondary ion mass spectrometry. *J. Anal. At. Spectrom.* **28**, 67–76.

MacPherson G. J., Davis A. M. and Zinner E. K. (1995) The distribution of aluminum-26 in the early solar system—a reappraisal. *Meteoritics* **30**, 365–386.

MacPherson G. J., Kita N. T., Ushikubo T., Bullock E. S. and Davis A. M. (2012) Well-resolved variations in the formation ages for Ca-Al-rich inclusions in the early solar system. *Earth Planet. Sci. Lett.* **331–332**, 43–54.

Maréchal C. N., Télouk P. and Albarède F. (1999) Precise analysis of copper and zinc isotopic compositions by plasma-source mass spectrometry. *Chem. Geol.* **156**, 251–273.

Matsuhisa Y., Goldsmith J. R. and Clayton R. N. (1978) Mechanisms of hydrothermal crystallization of quartz at 250°C and 15 kbar. *Geochim. Cosmochim. Acta* **42**, 173–182.

McKeegan K. D., Davis A. M., Taylor D. J. and MacPherson G. J. (2005) In-situ investigation of Mg isotope compositions in a FUN inclusion. *Lunar Planet. Sci.* **36**, #2077.

Mendybaev R. A., Richter F. M., Georg R. B., Janney P. E., Spicuzza M. J., Davis A. M. and Valley J. W. (2013) Experimental evaporation of Mg- and Si-rich melts: implications for the origin and evolution of FUN CAIs. *Geochim. Cosmochim. Acta* **123**, 368–384.

Mishra R. K. and Chaussidon M. (2014) Timing and extent of Mg and Al isotopic homogenization in the early inner solar system. *Earth Planet. Sci. Lett.* **390**, 318–326.

Nichols R. H. Jr., Wasserburg G. J., and Grimley R. T. (1995) Evaporation of forsterite: identification of gas-phase species via Knudsen cell mass spectrometry. *Lunar Planet. Sci.* **26**, 1047–1048.

Olsen M. B., Schiller M., Krot A. N., and Bizzarro M. (2013) Magnesium isotope evidence for single stage formation of CB chondrules by colliding planetesimals. *Astrophys. J.* **776**, L1 (6 pp).

Papineau D., Mojzsis S. J., Coath C. D., Karhu J. A. and McKeegan K. D. (2005) Multiple sulfur isotopes of sulfides from sediments in the aftermath of Paleoproterozoic glaciations. *Geochim. Cosmochim. Acta* **69**, 5033–5060.

Richter F. M. (2004) Timescales determining the degree of kinetic isotope fractionation by evaporation and condensation. *Geochim. Cosmochim. Acta* **68**, 4971–4992.

Richter F. M., Davis A. M., Ebel D. S. and Hashimoto A. (2002) Elemental and isotopic fractionation of Type B calcium-, aluminum-rich inclusions: experiments, theoretical considerations, and constraints on their thermal evolution. *Geochim. Cosmochim. Acta* **66**, 521–540.

Richter F. M., Janney P. E., Mendybaev R. A., Davis A. M. and Wadhwa M. (2007) Elemental and isotopic fractionation of Type B CAI-like liquids by evaporation. *Geochim. Cosmochim. Acta* **71**, 5544–5564.

Russell W. A., Papanastassiou D. A. and Tombrello T. A. (1978) Ca isotope fractionation on the Earth and other solar system materials. *Geochim. Cosmochim. Acta* **42**, 1075–1090.

Schramm D. N., Tera F. and Wasserburg G. J. (1970) The isotopic abundance of ^{26}Mg and limits on ^{26}Al in the early solar system. *Earth Planet. Sci. Lett.* **10**, 44–59.

961 Shahar A. and Young E. D. (2007) Astrophysics of CAI formation as revealed by silicon isotope
962 LA-MC-ICPMS of an igneous CAI. *Earth Planet. Sci. Lett.* **257**, 497–510.

963 Simon J. I., Young E. D., Russell S. S., Tonui E. K., Dyl K. A. and Manning C. E. (2005) A
964 short timescale for changing oxygen fugacity in the solar nebula revealed by high-resolution
965 ^{26}Al-^{26}Mg dating of CAI rims. *Earth Planet. Sci. Lett.* **238**, 272–283.

966 Teng F.-Z., Li W.-Y., Ke S., Marty B., Dauphas N., Huang S., Wu F.-Y. and Pourmand A.
967 (2010) Magnesium isotopic composition of the Earth and chondrites. *Geochim. Cosmochim.*
968 *Acta* **74**, 4150–4166.

969 Thrane K., Bizzarro M. and Baker J. A. (2006) Extremely brief formation interval for refractory
970 inclusions and uniform distribution of ^{26}Al in the early solar system. *Astrophys. J.* **646**,
971 L159–L162.

972 Villeneuve J., Chaussidon M. and Libourel G. (2009) Homogeneous distribution of ^{26}Al in the
973 solar system from the Mg isotopic composition of chondrules. *Science* **325**, 985–988.

974 Wang J., Davis A. M., Clayton R. N. and Hashimoto A. (1999) Evaporation of single crystal for-
975 sterite: evaporation kinetics, magnesium isotope fractionation, and implications of mass-
976 dependent isotopic fractionation of a diffusion-controlled reservoir. *Geochim. Cosmochim.*
977 *Acta* **63**, 953–966.

978 Wang J., Davis A. M., Clayton R. N., Mayeda T. K. and Hashimoto A. (2001) Chemical and iso-
979 topic fractionation during the evaporation of the FeO-MgO-SiO_2-CaO-Al_2O_3-TiO_2 rare earth
980 element melt system. *Geochim. Cosmochim. Acta* **65**, 479–494.

981 Wang M., Audi G., Wapstra A. H., Kondev F. G., MacCormick M., Xu X., and Pfeiffer B.
982 (2012) The AME2012 atomic mass evaluation (II). Tables, graphs, and references. *Chinese*
983 *Phys. C* **36**, 1603–2014.

984 Wasserburg G. J., Lee T. and Papanastassiou D. A. (1977) Correlated O and Mg isotopic anoma-
985 lies in Allende inclusions: II. Magnesium. *Geophys. Res. Lett.* **4**, 299–302.

986 Wasserburg G. J., Wimpenny J., and Yin Q.-Z. (2012) Mg isotopic heterogeneity, Al-Mg
987 isochrons, and canonical ^{26}Al/^{27}Al in the early solar system. *Meteorit. Planet. Sci.* **47**, 1980–
988 1997.

989 Wombacher F. and Rehkämper M. (2003) Investigation of the mass discrimination of multiple
990 collector ICP-MS using neodymium isotopes and the generalized power law. *J. Anal. At.*
991 *Spectrom.* **18**, 1371–1375.

992 Young E. D. and Galy A. (2004) The isotope geochemistry and cosmochemistry of magnesium.
993 *Rev. Mineral. Geochem.* **55**, 197–230.

994 Young E. D., Galy A. and Nagahara H. (2002) Kinetic and equilibrium mass-dependent isotope
995 fractionation laws in nature and their geochemical and cosmochemical significance.
996 *Geochim. Cosmochim. Acta* **66**, 1095–1104.

997 Young E. D., Simon J. I., Galy A., Russell S. S., Tonui E. and Lovera O. (2005) Supra-canonical
998 ^{26}Al/^{27}Al and the residence time of CAIs in the solar protoplanetary disk. *Science* **308**, 223–
999 227.

1000 Zhang J., Huang S., Davis A. M., Dauphas N., Jacobsen S. B., & Hashimoto A. (2014) Calcium
1001 and titanium isotopic fractionations during evaporation. *Geochim. Cosmochim. Acta* **140**,
1002 365–380.

1003 Zinner E. (2014) Presolar grains. In *Meteorites and Cosmochemical Processes* (Ed. A. M. Da-
1004 vis), Vol. 1 *Treatise on Geochemistry, 2nd Ed.* (Exec. Eds. H. D. Holland and K. K.
1005 Turekian), Elsevier, Oxford, pp. 181–213.

Table 1. Magnesium isotopic compositions of CAI-like evaporation residues produced in a vacuum furnace at 1600–1900°C. Uncertainties are 2σ and are based on the larger of the external and internal reproducibility (see text).

	% Mg evap	δ^{25}Mg (‰)	δ^{26}Mg (‰)	δ^{25}Mg (‰)	δ^{26}Mg (‰)
		"locally" normalized to daily R-13		"globally" normalized to all R-13	
Starting material					
Start	0	0.008 ± 0.097	–0.011 ± 0.175	–0.034 ± 0.097	0.009 ± 0.175
1900°C					
R3-10	42.59	8.150 ± 0.084	15.948 ± 0.152	8.107 ± 0.084	15.968 ± 0.152
R3-11	82.61	25.858 ± 0.084	51.042 ± 0.152	25.814 ± 0.084	51.063 ± 0.152
R3-9	94.99	43.344 ± 0.084	86.169 ± 0.152	43.300 ± 0.084	86.190 ± 0.152
R3-15	96.15	47.821 ± 0.084	95.296 ± 0.152	47.776 ± 0.084	95.318 ± 0.152
1800°C					
R13	0	0.000 ± 0.029	0.002 ± 0.052	≡0.000 ± 0.029	≡0.000 ± 0.052
R6	–0.27	0.133 ± 0.084	0.336 ± 0.152	0.209 ± 0.084	0.444 ± 0.152
R8	7.02	0.938 ± 0.084	1.970 ± 0.152	1.015 ± 0.084	2.083 ± 0.152
R3	11.47	1.726 ± 0.084	3.304 ± 0.152	1.766 ± 0.084	3.369 ± 0.152
R9	23.02	3.550 ± 0.084	7.000 ± 0.152	3.632 ± 0.084	7.131 ± 0.152
R2	33.86	5.503 ± 0.084	10.913 ± 0.152	5.613 ± 0.084	10.983 ± 0.152
R11	42.23	7.703 ± 0.060	15.065 ± 0.107	7.660 ± 0.060	15.085 ± 0.107
R7	54.11	10.583 ± 0.064	20.967 ± 0.115	10.685 ± 0.064	21.100 ± 0.115
R18	71.21	17.062 ± 0.075	33.629 ± 0.136	17.168 ± 0.075	33.854 ± 0.136
R4	74.94	18.713 ± 0.084	37.128 ± 0.152	18.824 ± 0.084	37.199 ± 0.146
R2-4	72.82	18.882 ± 0.083	37.236 ± 0.115	18.992 ± 0.084	37.403 ± 0.115
R3-14	83.41	25.418 ± 0.084	50.126 ± 0.152	25.375 ± 0.084	50.147 ± 0.152
R2-1	99.12	69.151 ± 0.084	139.006 ± 0.152	69.350 ± 0.084	139.604 ± 0.152
1700°C					
R2-21	1.39	0.210 ± 0.084	0.466 ± 0.152	0.250 ± 0.084	0.531 ± 0.152
R2-10	37.93	6.257 ± 0.091	12.092 ± 0.152	6.298 ± 0.091	12.158 ± 0.152
R2-18	69.97	15.688 ± 0.103	30.783 ± 0.175	15.729 ± 0.097	30.850 ± 0.175
R2-11	72.47	16.428 ± 0.097	32.563 ± 0.175	16.539 ± 0.097	32.634 ± 0.175
R2-20	79.81	20.610 ± 0.084	40.665 ± 0.152	20.651 ± 0.084	40.733 ± 0.152
R2-12	93.35	35.073 ± 0.116	69.587 ± 0.152	35.079 ± 0.116	69.656 ± 0.152
1600°C					
R3-2	0.00	–0.105 ± 0.084	–0.259 ± 0.152	–0.147 ± 0.084	–0.240 ± 0.152
R3-1	42.07	6.200 ± 0.084	12.138 ± 0.152	6.157 ± 0.084	12.158 ± 0.152
R3-19	63.31	11.908 ± 0.084	23.388 ± 0.152	11.949 ± 0.084	23.454 ± 0.152
R3-20	65.10	12.359 ± 0.084	24.353 ± 0.152	12.399 ± 0.084	24.419 ± 0.152
R3-18	77.74	17.978 ± 0.084	35.444 ± 0.175	18.019 ± 0.097	35.511 ± 0.175
R3-4	75.93	19.897 ± 0.084	39.097 ± 0.152	19.854 ± 0.084	39.118 ± 0.152
R3-8	92.15	32.419 ± 0.084	64.201 ± 0.152	32.375 ± 0.084	64.222 ± 0.152

1047

1048

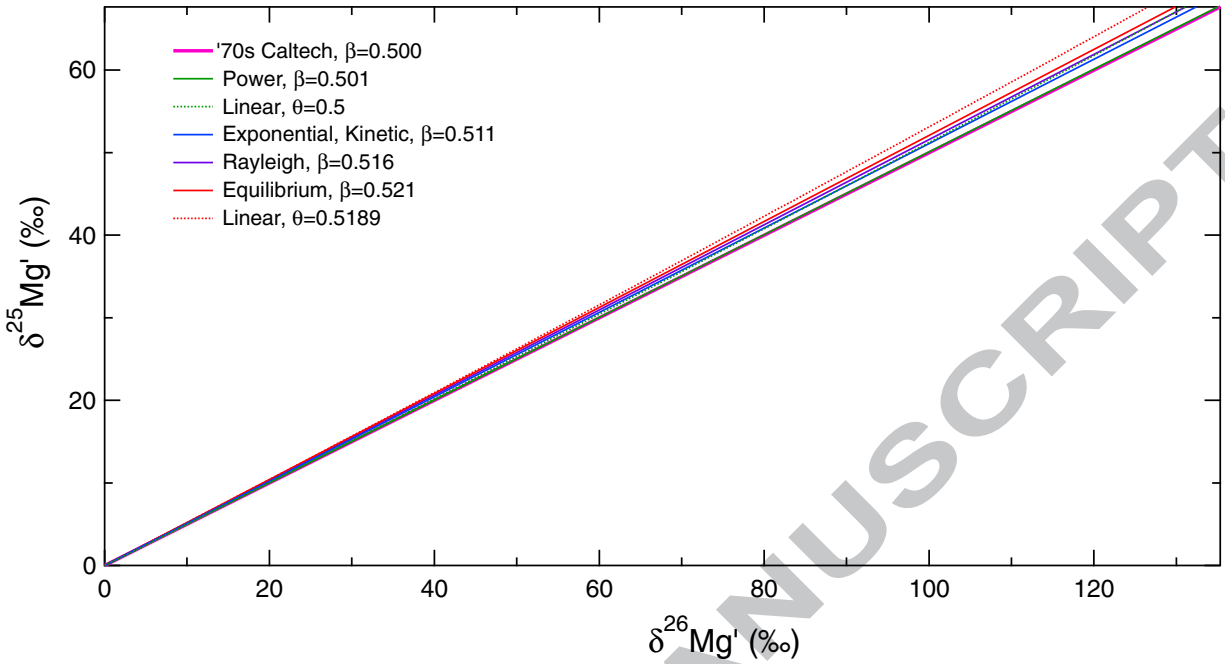

1049

1050 Figure 1. The relationship between $\delta^{25}Mg'$ and $\delta^{26}Mg'$ depends on the mass fractionation law
1051 governing the fractionation. All but the "Linear" lines are straight on this plot.
1052

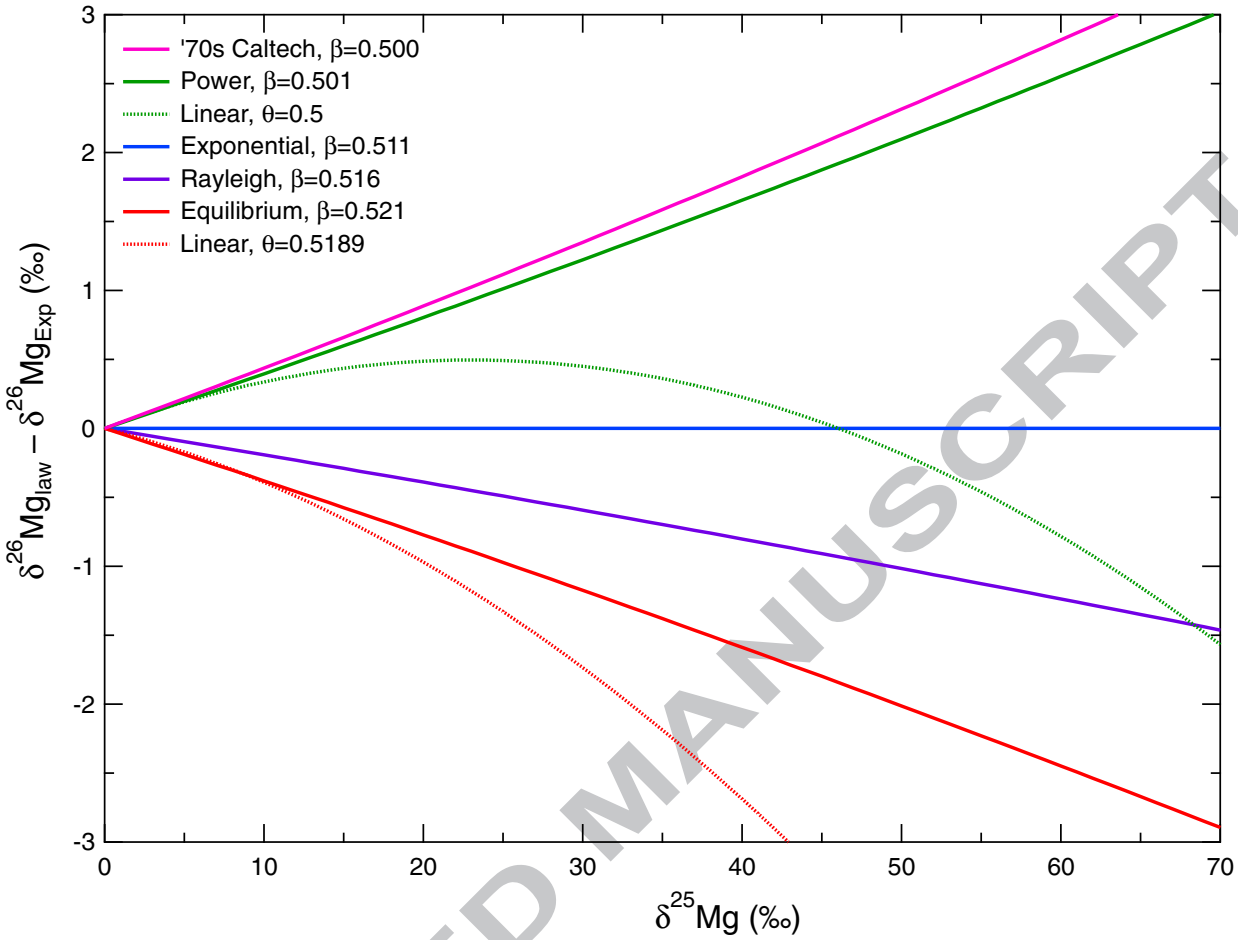

Figure 2. Differences in slope on Fig. 1 can be seen more easily when the differences between fractionation laws are plotted vs. degree of mass fractionation, here expressed as δ^{25}Mg. On this plot, the Rayleigh, power, exponential, kinetic and equilibrium laws are nearly linear and linear fractionation laws show considerable curvature.

1059

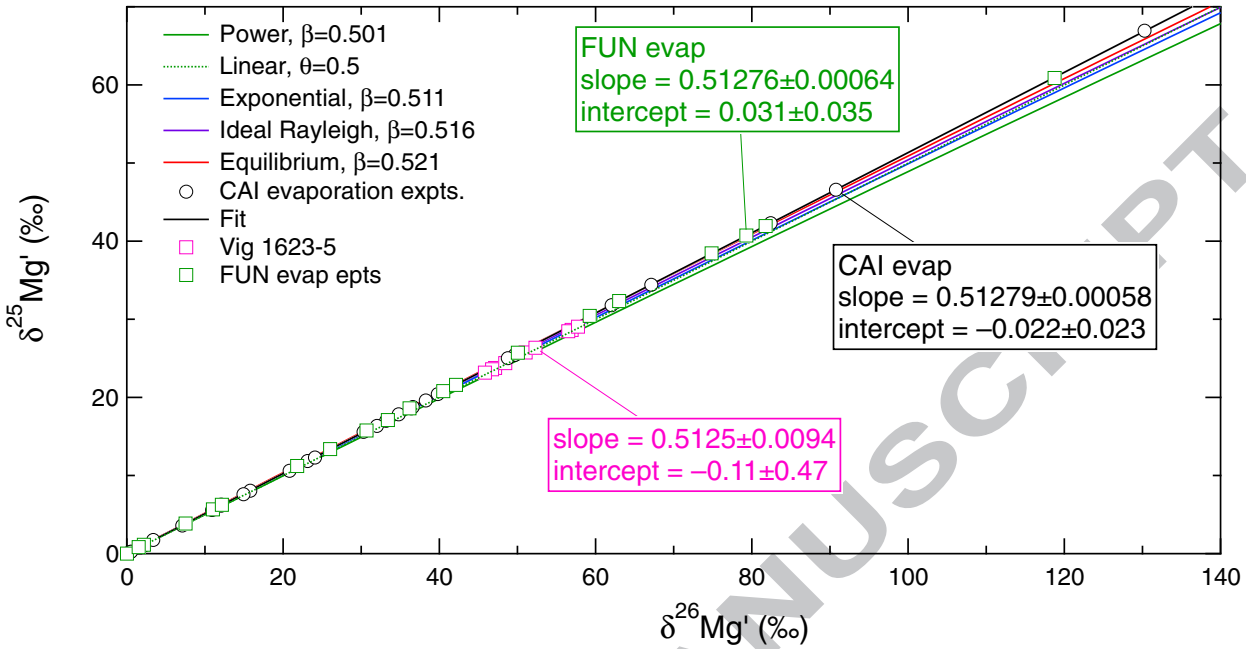

1060

1061 Figure 3. Relationships between $\delta^{25}Mg'$ and $\delta^{26}Mg'$ measured in evaporation residues and in
1062 forsterite from the FUN CAI Vigarano 1623-5 are compared with various fractiona-
1063 tion laws. All but the "Linear" lines are straight on this plot.
1064

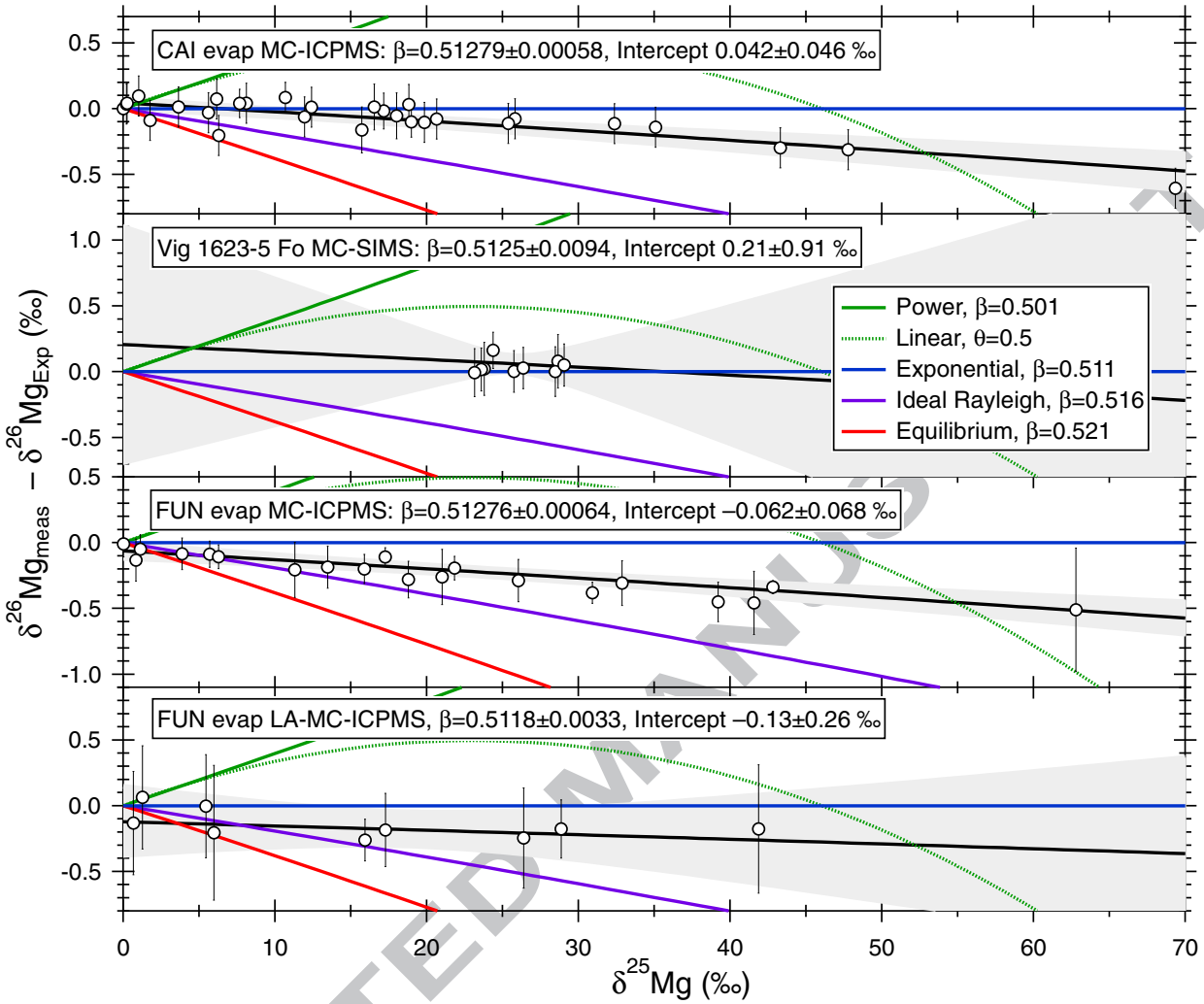

Figure 4. Differences between mass fractionation laws vs. δ^{25}Mg are plotted for: (1) CAI evaporation residues, measured by solution MC-ICPMS; (2) forsterite from the FUN CAI Vigarano 1623-5, measured by MC-SIMS; (3) forsterite-rich FUN CAI evaporation experiments of Mendybaev et al. (2013), measured by solution MC-ICPMS; and (4) forsterite-rich FUN CAI evaporation experiments of Mendybaev et al. (2013), measured by laser ablation MC-ICPMS. The shading shows the 2σ error bounds for the fits through the data in each panel. The Vigarano data are permissive of either the exponential/kinetic law or the experimentally determined law, but not the equilibrium law. The two sets of evaporation experiments, CAI and FUN are in excellent agreement and indicate that the fractionation law is not strongly dependent on melt composition.